frontiers | Frontiers in Earth Science

TYPE Original Research
PUBLISHED 19 May 2025
DOI 10.3389/feart.2025.1592749

Check for updates

OPEN ACCESS

EDITED BY
Xiaoguang Liu,
Shandong University of Science and Technology, China

REVIEWED BY
Yi Shi,
University of South China, China
Rongrong Guo,
Chengdu University, China

*CORRESPONDENCE
Linchuan Li,
lilinchuan@mail.cgs.gov.cn

RECEIVED 13 March 2025
ACCEPTED 30 April 2025
PUBLISHED 19 May 2025

CITATION
Chen J, Li L, Li B, Tian Y, Zhang C, Zang Y and Zhao Y (2025) Genesis and geological significance of the mafic rocks in the paleoproterozoic Lieryu formation, Liaoning. *Front. Earth Sci.* 13:1592749.
doi: 10.3389/feart.2025.1592749

Genesis and geological significance of the mafic rocks in the paleoproterozoic Lieryu formation, Liaoning

Jingsheng Chen[1,2,3], Linchuan Li[1,2,3]*, Bin Li[1,2,3], Yi Tian[4], Chao Zhang[1,2,3], Yanqing Zang[1,2,3] and Yan Zhao[1,2,3]

[1]Shenyang Geological Survey Center of China Geological Survey, Shenyang, China, [2]Northeast Geological S&T Innovation Center of China Geological Survey, Shenyang, China, [3]Geological Research Center of Eastern Continental Edge, China Geological Survey, Shenyang, China, [4]Liaoning Geological and Mineral Survey Institute Co., Ltd., Shenyang, China

Introduction: The Jiao-Liao-Ji Belt (JLJB), situated between the Longgang Block and Nangrim Block, hosts extensive Paleoproterozoic metasedimentary-volcanic sequences of the Liaohe Group. There has always been controversy over the stratigraphic relationships between the various formations of the Liaohe Group and the tectonic evolution of the JLJB.

Methods: Field investigations, petrology, zircon U-Pb dating, and whole-rock geochemistry.

Results: The mafic rocks from the Lieryu Formation comprises gabbro and amphibolites. Zircon U-Pb geochronology yields crystallization ages of ca. 2052 ± 15 Ma, 2089 ± 55 Ma, 2053 ± 28 Ma, and 2,190 ± 13 Ma, which reconstruct the geochronological framework of Lieryu mafic magmatism to 2,190–1995 Ma. The average SiO_2 content of samples ranges from 48.11 wt% to 50.47 wt%, which indicates mafic rocks. The K_2O content of samples varies from 0.81 wt% to 1.44 wt% respectively, indicating calc-alkaline to high-K calc-alkaline series. The value of $Mg^{\#}$ ranges from 45.93 to 57.10.

Discussion: The chronology of volcanic rocks cross different formations of the Liaohe Group exhibiting no systematic stratigraphic progression but rather interfingering relationships. Combined with field observations of mélange associated with boron deposits within the Lieryu Formation, it is believed that the Liaohe Group is not coherent stratigraphic succession, but a disordered tectonic stratigraphic unit. The results of trace element show that the Paleoproterozoic mafic rocks originated from a transitional mantle source, and three of them (D1902, D1905 and D1911) are mainly influenced by metasomatism, while the D1914 influenced by dual fluid and melt in the source. The D1902, D1905 and D1914 are product of partial melting of amphibole-bearing spinel lherzolite, leading to residual hornblende and spinel in the source. The D1911 is from partial melting of garnet–spinel lherzolite with the 50:50 ratios of garnet and spinel and 6:1 ratio of clinopyroxene to garnet, resulting in garnet and spinel left in the source. During the ascent and emplacement, assimilation and contamination occurred between mafic magmas and continental crustal materials. Geochemical data from the Lieryu mafic rocks reveal that D1902 (amphibolite) and D1914 (gabbro) show the same characteristics with island arc basalt (IAB), indicating an island arc environment. D1905 (amphibolite) and D1911 (gabbro) show the same characteristics with mid-ocean ridge basalt (MORB), and were formed in a mid-ocean ridge environment. These evidences indicate an ancient ocean existed in the Paleoproterozoic. The JLJB represents a collisional orogen formed during the closure of the Paleoproterozoic oceanic basin.

KEYWORDS

Paleoproterozoic mafic rocks, Lieryu formation, Zircon U-Pb chronology, geochemistry, feature of source, tectonic background

1 Introduction

The North China Craton (NCC) is one of the important Archean cratons in the eastern part of the Eurasian Continent. In recent years, significant progresses have been achieved on Paleoproterozoic tectonic evolution of the NCC, suggesting the existence of three Paleoproterozoic orogenic belts (Zhao et al., 2005; 2012; Zhao and Zhai, 2013), among which the Jiao-Liao-Ji Belt (JLJB) is currently the only widely accepted Paleoproterozoic orogenic belt. This orogenic belt is widely distributed in the Liaodong region and is known as the Liao-Ji tectonic belt. It is a Paleoproterozoic orogenic belt that connects the Liaonan-Nangrim Block in southern Liaoning and the Longgang Block in northern Liaoning-southern Jilin Province (Zhao et al., 2005; 2012) (Figure 1a). As an important carrier for studying the Paleoproterozoic tectonic evolution, all the Pre-Cambrian magmatic-sedimentary events have been completely preserved in the JLJB. Many research progress have been obtained on its material composition (Liu et al., 2015), sedimentation (Luo et al., 2008; Li et al., 2015a; b; Zhang et al., 2018), magmatism (Li and Zhao, 2007; Meng et al., 2014; Chen et al., 2017a; 2017b; Xu et al., 2017; 2018a; 2018b; Zhao et al., 2019), metamorphism (Liu et al., 2017; 2019), tectonism (Li et al., 2005; Tian et al., 2017), and tectonic evolution (Bai, 1993; Zhao and Zhai, 2013; Xu and Liu, 2019). However, there are still two issues of debate regarding the study of the JLJB.

The first issue is whether the Lieryu Formation in the South Liaohe Group constitutes an ordered stratigraphic sequence. The Paleoproterozoic layered metamorphic sedimentary-volcanic rocks in this region are referred to as the North and South Liaohe Group in Liaoning, while in Jilin, they are known as the Laoling Group and Ji'an Group (Liu et al., 2015). There are different opinions among scholars regarding the relationship between these various rock formations within it. Early researchers posited that the Liaohe Group represents an ordered stratigraphic sequence, divided from bottom to top into the Langzishan, Lieryu, Gaojiayu, Dashiqiao, and Gaixian Formations, formed through successive depositional events during the Paleoproterozoic era (Bureau of Geology and Mineral Resource of Liaoning Province, 2014). However, recent regional geological surveys and in-depth studies on the Liaohe Group have led some scholars to propose alternative perspectives. Based on field observations and the geochronological characteristics of felsic volcanic rocks from the Lieryu Formation, the Liaohe Group is considered to be a disordered tectonic stratigraphic unit, with no clear conformable relationships among its formations (Li et al., 2015a; b; Liu et al., 2015; Chen et al., 2017a; 2018; 2020a; 2020b; 2021; 2024). In recent geological surveys, in addition to "bedded" amphibolite, marble, and granulite there is also a suite of mafic-ultramafic rocks associated with boron deposits have been observed in the Lieryu Formation from the Liaohe Group. These rocks include peridotite, gabbro, tourmaline granulite, and plagiogranite, occurring as a mélange, which further supports the possibility that the Lieryu Formation may not represent an ordered stratigraphic sequence.

The second issue is that there are still differences among scholars on the tectonic evolution model of the JLJB. The existing evolutionary model can be summarized as follows: (1) Continental rift opening-closure model: Scholars who hold this view believe that this belt was formed through the initial rifting and subsequent sedimentation of a continental rift, followed by recombination through subduction and collision (Zhang and Yang, 1988; Li et al., 2006; Zhao et al., 2005; 2011; 2012; Zhao and Zhai, 2013; Zhai and Santosh, 2011). (2) Subduction-accretion model: Some scholars, integrating modern plate tectonic theory and evidence from petrology, structure and paleogeothermal studies, propose that the belt represents a continent-arc collision zone formed through island arc accretion. Some researchers suggest that the orogenic belt is developed due to the closure of a back-arc basin (Bai, 1993; Li and Chen, 2014; Li et al., 2015a; Li et al., 2015b; Li et al., 2019a; Li et al., 2015b; Lu et al., 2006; Meng et al., 2014), with magmatic activity recording a complete tectonic cycle, including oceanic subduction, back-arc extension, back-arc basin closure, collisional orogeny, and post-collisional extension (Xu and Liu, 2019). The other researchers, supporting this model, believe that the orogenic belt formed through a complete Wilson cycle, encompassing Paleoproterozoic rifting, extension, ocean basin formation, subduction, and collision (Zhao et al., 2012; 2013; Zhai and Santosh, 2011; 2013; Li et al., 2012). (3) Continent-continent collision model: Based on the differing metamorphic grades and contrasting P-T-t evolution paths observed in the North Liaohe Group (Laoling Group) and South Liaohe Group (Ji'an Group), some scholars infer that these rock units originated from distinct continental blocks that collided and amalgamated during the Paleoproterozoic (Lu, 1996; He and Ye, 1998; Li et al., 2001).

The Lieryu Formation is characterized by extensive exposures of both felsic volcanic rocks and mafic rocks (including amphibolite, gabbro, and peridotite). Previous studies have mostly focused on the felsic volcanic rocks (Chen et al., 2017a; 2017b; Bi et al., 2018a; 2018b), but limited research on mafic rocks (Chen et al., 2020a; 2020b). Mafic magmas, originating from the subcontinental asthenosphere or lithospheric mantle under continental extension, record significant geological events and play a crucial role in reconstructing craton tectonic evolution (Mo, 2019). They can be

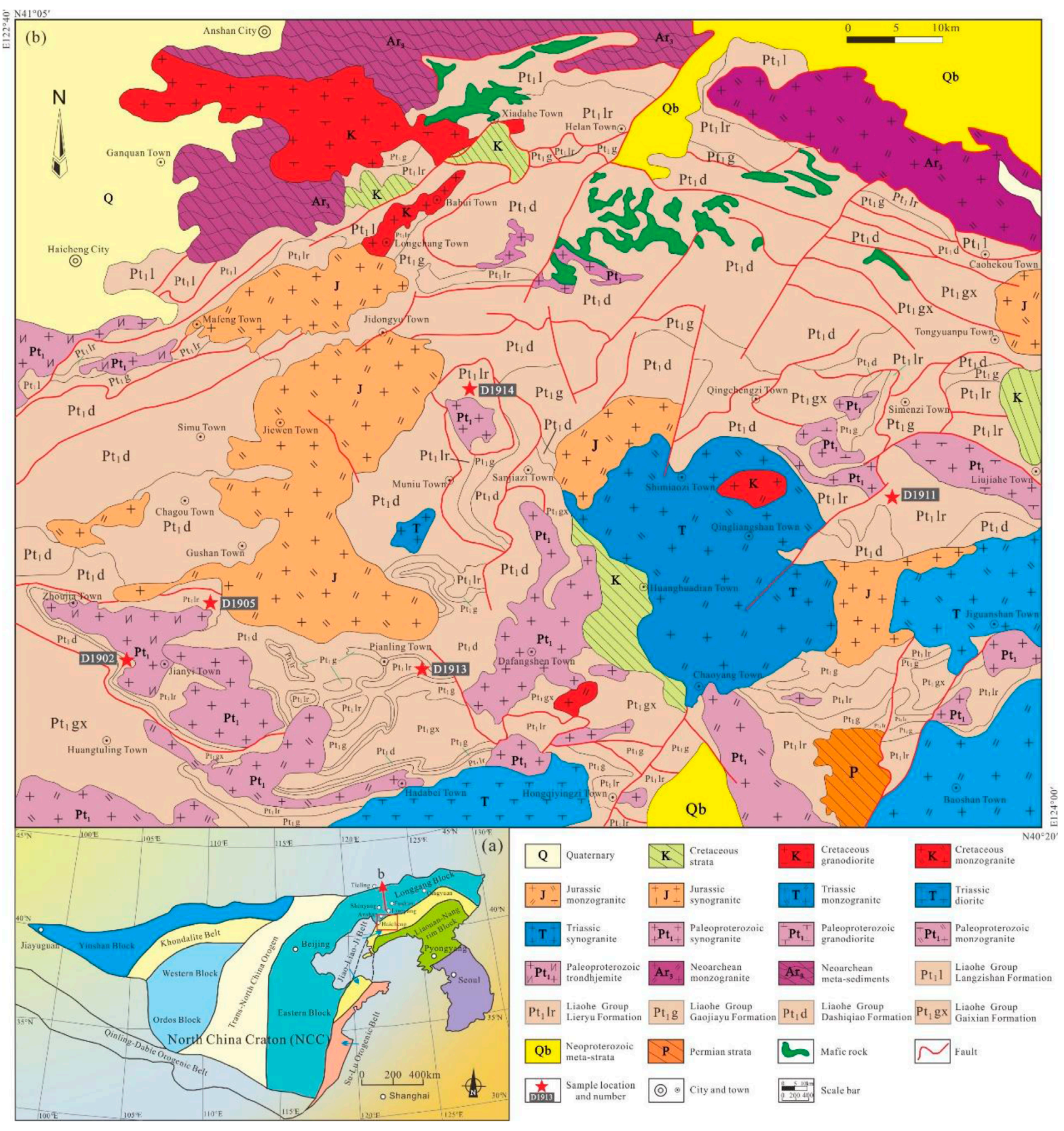

FIGURE 1
The tectonic location **(a)** (modified after Zhao et al., 2005); simplified geological map and sample location of the mafic rocks from the Lieryu Formation **(b)**.

used to study the characteristics of magma source, and the tectonic setting. So, the mafic rocks from the Lieryu Formation are the key to discuss the tectonic evolution of JLJB. So, the newly identified mafic rocks including amphibolite and gabbro were selected, petrographic, geochronological, and geochemical studies on these mafic rocks were conducted to determine the tectonic feature of the Lieryu Formation and discuss tectonic evolution of JLJB in this area.

2 Geological setting and sample descriptions

2.1 Geological setting

The Liaodong region is part of NCC and has experienced all geological events from the Archean, Proterozoic, Paleozoic, Mesozoic to Cenozoic. It mainly exhibits Archean crystalline basement, Paleoproterozoic orogenic belt, and Triassic-Cretaceous intrusive rocks formed during the destruction of the NCC. The Precambrian basement is composed of the Archean Liaonan–Nangrim Block in the southeast and the Longgang Block in the northwest, and the Paleoproterozoic JLJB in the middle (Figure 1A; Zhang, 1988). Extensive occurrences of tonalite-trondhjemite- granodiorite rocks (TTGs) (Li et al., 2019a; b, 2020; Peng et al., 2015) and mafic volcanic rock (Li and Wei, 2017) exhibit in the Longgang Block, including approximately 3.8 Ga rocks and various ≥3.0 Ga zircons exposed in the Anshan area (Wan et al., 2005). Archean granitoid rocks have been observed in the Liaonan-Nangrim Block (Zhao et al., 2006).

The Paleoproterozoic JLJB, located between these two blocks, is characterized by large-scale distribution of meta-volcano-sedimentary successions and granitic to mafic intrusions (Xu et al., 2018a; 2018b; Xu and Liu, 2019; Liu et al., 2015; Chen et al., 2017a; 2018; 2020a; 2020b; 2021; 2024). Based on the degree of metamorphism and rock composition, along the Gaixian-Ximucheng-Taziling-Aiyang, the meta-sedimentary and volcanic rocks are divided into the South Liaohe Group and Ji'an Group on the south side, and the North Liaohe Group and Laoling Group on the north side, which have undergone low greenschist to amphibolite facies metamorphism (Bai, 1993; Li and Zhao, 2007; Liu et al., 2015; Liu et al., 2017; 2019). There are also Paleoproterozoic granitic rocks and metamorphic mafic intrusive rocks collectively known as "Liaoji granite" within the JLJB. The granitic rocks include striated or gneiss granite, porphyritic garnet monzogranite, and alkaline syenite (Li and Zhao, 2007; Liu et al., 2015; Chen et al., 2021).

The lithology of the Lieryu Formation is mainly composed of metamorphic rhyolite-decite interbedded with basalt, granulite, albite granulite, magnetite granulite, biotite granulite interbedded with amphibolite, and boron-bearing serpentine marble (Bureau of Geology and Mineral Resource of Liaoning Province, 2014). In recent years, according to 1:50,000 regional geological surveys and special studies in the Liaodong area, a rock complex related to boron deposits has been identified in the Lieryu Formation of the South Liaohe Group. The rock types include gabbro, peridotite, marble, and plagioclase granite, whose occurrence shows in the form of "blocks". This study focuses on the amphibolite and gabbro, identified from the Lieryu Formation. Geochronology and geochemistry were conducted on these sample to provide a basis for the structural properties of the JLJB.

2.2 Petrological characteristics of mafic rocks

In this study, 5 chronological samples and 24 geochemical samples of mafic rocks were collected from the Lieryu Formation for analysis, respectively. The sampling locations are shown in Figure 1b.

Sample D1902 is an amphibolite, collected from the Lieryu Formation located 5 km west of Jianyi Town (Figure 1b), intruded by later Paleoproterozoic granite (Figure 2a). It exhibits a crystalloblastic texture and a massive structure. The mainly mineral components include plagioclase (~30%), hornblende (~65%), and sphene (~5%), with obvious sericitization. Hornblende is subhedral and plate-columnar-shaped, displaying a yellow-green to green interference color, with typical cleavage of amphibole. Its grain size ranges from 0.2 to 1 mm. Plagioclase shows subhedral to anhedral columnar-shaped, exhibiting polysynthetic twin with slight sericitization, with grain size ranging from 0.2 to 0.5 mm. Sphene is anhedral granular texture, featuring a medium to high protrusion with advanced white interference colors, with grain size of 0.1–0.5 mm (Figures 2b,c). The accessory mineral is magnetite, with grain size of 0.05–0.1 mm, comprising approximately 1%.

Sample D1905, amphibolite, sourced from the Lieryu Formation, 7 km south of Gushan Town (Figure 1b). It is intruded by later felsic dike (Figure 2e). It is composed of minerals such as hornblende (~60%), plagioclase (~30%) biotite (~6%) and sphene (~3%) exhibiting crystalloblastic texture with foliated structure (Figure 2F). Hornblende appears subhedral and plate-columnar-shaped, yellow-green to green interference color, oriented along its long axis with a foliated structure and a particle size of 0.2–1 mm. Plagioclase is subhedral to anhedral columnar-shaped, showing polysynthetic twin with slight sericitization, with a grain size of 0.2–0.5 mm. Biotite, euhedral, brown in color, and is oriented in a foliated plane, ranging from 0.1 to 0.5 mm in diameter. Sphene shows anhedral granular texture, exhibiting a medium to high protrusion and advanced white interference colors, ranging from 0.1 to 0.5 mm in diameter. The magnetite, as accessory mineral, exhibits a particle size of 0.05–0.1 mm and a content of about 1% (Figures 2g,h).

Sample D1911 is a gabbro collected from the Nuanhe Boron Mine, located 12 km west of Liujiahe Town (Figure 1b). It exhibits a crystalblastic texture and a massive structure (Figures 2i,j). The mineral components are pyroxene (50%), plagioclase (40%), and biotite (10%), with sericite as the alteration mineral. The colorless to light green pyroxene is subhedral and plate-columnar-shaped, with typical cleavage of pyroxene, forming dark layers with biotite, and its grain size ranges from 0.2 to 2 mm. Subhedral and plate-columnar-shaped plagioclase shows polysynthetic twin with slight sericitization, often forms light-colored bands, with a diameter ranging from 0.2 to 1 mm. The euhedral biotite is light yellow to yellow in color, and forms dark layers with pyroxene, with a grain size of 0.2–2 mm (Figures 2k,l). Accessory minerals include small amounts of magnetite and others.

Sample D1913, amphibolite, is collected from the Lieryu Formation, 5 km east of Pianling Town (Figure 1b), showing a crystalloblastic texture and a massive structure (Figures 2q,r). The components include hornblende (50%), plagioclase (40%), epidote (7%), and quartz (3%), with notable sericitization and epidotization. Hornblende is subhedral and columnar, exhibiting a green to yellow-green color, and has a diameter of 0.2–1.6 mm. Plagioclase is also subhedral, showing polysynthetic twin with slight sericitization, with a grain size of 0.2–1.2 mm. Epidote is anhedral and granular, exhibiting positive high protrusion and abnormal interference colors, with a grain size of 0.1–0.4 mm. Quartz, with a grain size of 0.2–2.0 mm, is anhedral and granular (Figures 2s,t).

Sample D1914, hornblende gabbro, collected from 10 km southeast of Jidongyu Town (Figure 1b), exhibits a gabbroic texture and a massive structure (Figures 2m,n). The rock is composed of plagioclase (45%), pyroxene (50%), hornblende (4%), and biotite (1%), with alteration minerals including chlorite, sericite, and calcite. The plagioclase, subhedral columnar crystals ranging from

FIGURE 2
Occurrence and micro-pictures of mafic rocks from the Lieryu Formation. **(a–d)** D1902 amphibolite; **(a)** amphibolite xenolith in the granite; **(b)** fresh surface of the amphibolite; **(c,d)** microscopic characteristics of amphibolite; **(e–h)** D1905 amphibolite; **(e)** amphibolite is intruded by granite dike; **(F)** specimen of diabase; **(g,h)** microscopic characteristics of amphibolite; **(i–l)** D1911 gabbro; **(I)** gabbro is intruded by granite; **(j)** spherical weathering of gabbro; **(k,l)** microscopic characteristics of gabbro; **(m–p)** D1914 gabbro; **(m)** field occurrence of gabbro; **(n)** coarse-grained gabbro; **(o,p)** microscopic characteristics of gabbro; **(q–t)** D1913 amphibolite; **(q)** field occurrence of amphibolite; **(r)** spherical weathering of amphibolite; **(s,t)** microscopic characteristics of amphibolite; Pl: plagioclase; Px: pyroxene; Hbl: hornblende; Spn: sphene; Bt: biotite.

2 to 5 mm in diameter, shows polysynthetic twin and zoning, with slight sericitization along fractures. The light yellow to green pyroxene is subhedral and columnar, with slight carbonation and a dominant grain size of 1–2 mm. Hornblende is subhedral, exhibiting typical amphibole cleavage, and shows chloritization and carbonation with a few areas exhibiting reaction rims at the edges of pyroxene, and has a grain size of 0.5–2 mm. Biotite is euhedral, brown in color, with a grain size of 0.2–1 mm (Figures 2o,p). Accessory minerals include small amounts of magnetite and ilmenite.

3 Analytical methods

3.1 Sample preparation

After collection from the field, samples for geochronological analysis were cleaned, crushed, and ground. Zircon crystals were subsequently separated from these samples using conventional heavy liquid and magnetic techniques at Langfang Yuneng Mineral Separation Co., Ltd. in Langfang, China. The isolated zircons were carefully hand-picked under a binocular microscope. To investigate their internal structures, the selected zircons were embedded in epoxy resin, polished, and then imaged with a scanning electron microscope equipped with cathodoluminescence (CL) at Beijing Gaonian Navigation Technology Limited Company in Beijing, China. CL images of four samples were obtained using a CAMECA SX51 microprobe (manufactured by CAMECA in France), operating at 50 kV and 15 nA.

3.2 Zircon LA-ICP-MS U-Pb isotope dating

LA-ICP-MS U-Pb isotope analyses were conducted using an Agilent 7500a quadrupole ICP-MS (Agilent Technologies Co., Ltd) equipped with an UP-193 solid-state laser (193 nm, New Wave Research Inc., Shanghai). The laser spot size was set to 32 μm for most analyses, with a laser energy density of 10 J/cm^2 and a repetition rate of 8 Hz. The laser sampling procedure included a 30-s blank, followed by 30 s of sampling ablation, and a 2-min sample chamber flushing after ablation. The ablated material was transported to the ICP-MS by a high-purity helium gas stream with a flow rate of 1.15 L/min. The entire laser path was purged with argon (600 mL/min) to maintain energy stability. Counting times were 20 ms for isotopes ^{204}Pb, ^{206}Pb, ^{207}Pb, and ^{208}Pb; 15 ms for ^{232}Th and ^{238}U; 20 ms for ^{49}Ti; and 6 ms for other elements. NIST 610 glass served as an external standard, while Si was used as an internal standard for zircon analyses. U-Pb isotope fractionation effects were corrected using zircon 91,500 as an external standard (Wiedenbeck et al., 1995). Glitter software was used to calculate isotopic ratios and element concentrations of zircons (Ludwig, 2003). Concordia ages and diagrams were generated using Isoplot/Ex (3.0) (Ludwig, 2003). Common lead was corrected using the LA-ICP-MS Common Lead Correction (version 3.15), following the method of Andersen (2002). The analytical data are presented on U-Pb concordia diagrams with 1σ errors. Mean ages are reported as weighted means at 95% confidence intervals. The analyses of 5 samples were performed at the Key Laboratory of Mineral Resources Evaluation in Northeast Asia, Ministry of Natural Resources. The data are summarized in Table 1.

3.3 Major- and trace-element analyses

The major, trace, and rare earth element (REE) analyses results for 24 samples were obtained from the Northeast China Supervision and Inspection Center of Mineral Resources, Ministry of Natural Resources (Shenyang, China). After petrographic examination and the altered rock surfaces were removed, the samples were crushed and ground to 74 μm using an agate mill. X-ray fluorescence spectrometry (XRF) method was used for the major element contents of the whole rock, with analytical precisions exceeding 2%. X Series II ICP-MS was used for the trace element and REE contents testing. A total of 0.1 g of the sample was placed in a digestion tank, with 1 mL of concentrated nitric acid and 1 mL of hydrofluoric acid added. After placed in an oven, the digestion tank was heated up to 180° for 10–12 h. After removal, it was heated at 120° on an electric heating plate in an open environment. Until only 2–3 mL of the digestion solution was left, it was heated up to 240°. After redissolving, 0.5% dilute nitric acid was added to the mark for measurement. Twelve times measurements were conducted on samples, with analytical precisions exceeding 5% for elements with contents of >10 μg/g, exceeding 8% for elements with contents of <10 μg/g, and 10% for the transition metals. The results are listed in Supplementary Table S1.

4 Analytical results

4.1 Zircon U-Pb geochronology

Twelve isotopic analyses were conducted on zircons from sample D1902. They are mostly euhedral rhombohedral with diameters of 100–140 μm and length-width ratios of 1.5:1 to 2:1, generally black, but unclear internal texture (Figure 3). Light edges with different widths occurred around the most zircons, which may be the proliferative edges formed by recrystallization during metamorphism. The Th/U ratios are ranging from 0.75 to 1.96, which indicates a magmatic origin (Hoskin and Ireland, 2000; Belousova et al., 2002). Twelve analyses yield an upper intercept age of 2052 ± 15 Ma (n = 12, MSWD = 0.02), which is consistent with the ^{207}Pb/^{206}Pb weighted average age of 2056 ± 11 Ma (n = 4, MSWD = 0.82) from 4 zircons on the concordant line (Figure 4a). Thus, this result represents the magmatic crystallization age.

Twenty-five zircons have been chosen from D1905. In cathodoluminescence (CL) imaging, they are smaller in size with diameters of 40–70 μm and length-width ratios of 1:1 to 2:1, generally black mostly, without clear internal texture (Figure 3). Light secondary outgrowth rims with different widths occurred around all the zircons, which may be the product of recrystallization during metamorphism (Figure 3). Combining with high Th/U ratios (0.48–3.38), indicating zircons in this sample are magmatic-derived zircon (Hoskin and Ireland, 2000; Belousova et al., 2002). Twenty-five analyses yield an upper intercept age of 2089 ± 55 Ma (n = 25, MSWD = 5.8), which is consistence with the ^{207}Pb/^{206}Pb age (2088 ± 11 Ma) in the concordant line (Figure 4B). Thus, this age is interpreted as the time of magmatic emplacement.

Zircons from sample D1911 can be divided into two groups according to the CL images (Figure 3). The shape of first group zircons is sub-angular with grain size ranging from 80 μm to 110 μm and length/width ratios of 1:1–2.5:1. The black cores and gray rims are present in these grains with no obvious zoning. The ratios of Th/U range from 0.59 to 1.65, indicating a magmatic origin (Hoskin and Ireland, 2000; Belousova et al., 2002). Seven analysis were obtained from seven zircons, yielding a concordant ^{207}Pb/^{206}Pb age of 2053 ± 28 Ma (n = 7, MSWD = 9.8) (Figure 4d). This result is interpreted as the age of magma crystallization. Zircons from the second group is sub-rounded with size ranging from 50 μm to 120 μm and length/width ratios from 1:1–2.5:1. The white cores with unzoned internal texture (Figure 3) and low ratio of Th/U (0.05–0.10), indicating a metamorphic zircon (Hoskin and Ireland, 2000; Belousova et al., 2002). Seventeen analysis were obtained from seventeen zircons, yielding a concordant ^{207}Pb/^{206}Pb age of 1835 ± 13 Ma (n = 17, MSWD = 3.7) (Figure 4D). This result is interpreted as the time of later metamorphism.

In cathodoluminescence (CL) imaging, zircons from sample D1914 can be divided into three groups. The zircons of first group show large grain size with the diameter of 110–210 μm and

TABLE 1 LA-ICP-MS zircon U-Pb dating data of mafic rocks from the Lieryu Formation.

Sample no.	Pb	Th	U	Th/U	Isotopic ratios						Ages(Ma)					
	ppm	ppm	ppm		$^{207}Pb/^{206}Pb$		$^{207}Pb/^{235}U$		$^{206}Pb/^{238}U$		$^{207}Pb/^{206}Pb$		$^{207}Pb/^{235}U$		$^{206}Pb/^{238}U$	
					Ratio	1σ	Ratio	1σ	Ratio	1σ	Ages	1σ	Ages	1σ	Ages	1σ
D1902-1	294	490	563	0.87	0.12608	0.00214	6.50981	0.11098	0.37455	0.00448	2044	15	2047	15	2051	21
D1902-2	789	1,500	1,402	1.07	0.13337	0.00149	6.88934	0.08021	0.37471	0.00403	2,143	9	2097	10	2052	19
D1902-3	316	937	479	1.96	0.12632	0.00152	6.53444	0.08128	0.37523	0.00409	2047	10	2051	11	2054	19
D1902-4	621	1,114	1,134	0.98	0.13316	0.00151	6.90248	0.08145	0.37599	0.00405	2,140	9	2099	10	2058	19
D1902-5	658	1,245	1,201	1.04	0.13214	0.00146	6.83555	0.07864	0.37523	0.00402	2,127	9	2090	10	2054	19
D1902-6	1,199	3,551	1846	1.92	0.12308	0.00155	6.34986	0.08219	0.37420	0.00411	2001	10	2025	11	2049	19
D1902-7	992	3,033	1718	1.76	0.12975	0.00149	6.69617	0.07952	0.37431	0.00404	2095	9	2072	10	2050	19
D1902-8	576	1,170	1,044	1.12	0.12747	0.00137	6.60610	0.07393	0.37585	0.00400	2063	9	2060	10	2057	19
D1902-9	868	2,710	1,453	1.86	0.12938	0.00150	6.68642	0.07989	0.37479	0.00405	2090	9	2071	11	2052	19
D1902-10	224	322	429	0.75	0.13493	0.00153	6.96470	0.08185	0.37435	0.00403	2,163	9	2,107	10	2050	19
D1902-11	632	977	1,251	0.78	0.12758	0.00205	6.59254	0.10622	0.37474	0.00440	2065	14	2058	14	2052	21
D1902-12	657	1,278	1,205	1.06	0.12981	0.00138	6.72403	0.07434	0.37565	0.00399	2095	9	2076	10	2056	19
D1905-1	740	2,288	1,313	1.74	0.12247	0.00127	4.43496	0.04863	0.26287	0.00285	1993	9	1719	9	1,505	15
D1905-2	884	2,768	1875	1.48	0.12098	0.00123	4.60245	0.04970	0.27612	0.00299	1971	9	1750	9	1,572	15
D1905-3	453	1,119	954	1.17	0.11267	0.00116	3.22907	0.03509	0.20799	0.00225	1843	9	1,464	8	1,218	12
D1905-4	887	2,306	1795	1.28	0.11492	0.00116	3.37195	0.03626	0.21293	0.00229	1879	9	1,498	8	1,244	12
D1905-5	1,221	4,671	2,479	1.88	0.11742	0.00120	4.41548	0.04795	0.27286	0.00294	1917	9	1715	9	1,555	15
D1905-6	516	1,318	1,078	1.22	0.11558	0.00155	4.62834	0.06343	0.29053	0.00327	1889	11	1754	11	1,644	16
D1905-7	564	982	1,278	0.77	0.12316	0.00131	4.76432	0.05322	0.28064	0.00303	2003	9	1779	9	1,595	15
D1905-8	402	720	919	0.78	0.12335	0.00131	4.90139	0.05471	0.28826	0.00311	2005	9	1802	9	1,633	16

(Continued on the following page)

10.3389/feart.2025.1592749

TABLE 1 (*Continued*) LA-ICP-MS zircon U-Pb dating data of mafic rocks from the Lieryu Formation.

Sample no.	Pb	Th	U	Th/U	Isotopic ratios						Ages(Ma)					
	ppm	ppm	ppm		$^{207}Pb/^{206}Pb$		$^{207}Pb/^{235}U$		$^{206}Pb/^{238}U$		$^{207}Pb/^{206}Pb$		$^{207}Pb/^{235}U$		$^{206}Pb/^{238}U$	
					Ratio	1σ	Ratio	1σ	Ratio	1σ	Ages	1σ	Ages	1σ	Ages	1σ
D1905-9	337	676	905	0.75	0.12927	0.00167	6.85495	0.09116	0.38467	0.00433	2088	11	2093	12	2098	20
D1905-10	390	444	921	0.48	0.11754	0.00132	4.71548	0.05506	0.29099	0.00316	1919	9	1770	10	1,646	16
D1905-11	669	2,614	1,192	2.19	0.11724	0.00126	3.51237	0.03951	0.21727	0.00233	1915	9	1,530	9	1,267	12
D1905-12	1,001	4,825	2,485	1.94	0.11316	0.00117	3.37251	0.03658	0.21612	0.00231	1851	9	1,498	8	1,261	12
D1905-13	230	163	542	0.30	0.12342	0.00188	4.97807	0.07622	0.29248	0.00338	2006	13	1816	13	1,654	17
D1905-14	709	2,393	1,215	1.97	0.12055	0.00130	4.76789	0.05360	0.28680	0.00307	1964	9	1779	9	1,626	15
D1905-15	767	2,411	1,413	1.71	0.12202	0.00128	4.39966	0.04827	0.26144	0.00279	1986	9	1712	9	1,497	14
D1905-16	433	1725	694	2.48	0.12077	0.00126	4.25718	0.04637	0.25558	0.00271	1968	9	1,685	9	1,467	14
D1905-17	559	722	1,220	0.59	0.12033	0.00155	4.92397	0.06472	0.29667	0.00327	1961	11	1806	11	1,675	16
D1905-18	362	1,235	663	1.86	0.12079	0.00131	4.25181	0.04793	0.25520	0.00272	1968	9	1,684	9	1,465	14
D1905-19	692	2,355	1,291	1.82	0.12461	0.00169	4.29498	0.05911	0.24988	0.00278	2023	11	1,692	11	1,438	14
D1905-20	811	1981	1,593	1.24	0.11718	0.00125	4.32269	0.04795	0.26744	0.00284	1914	9	1,698	9	1,528	14
D1905-21	456	1,004	884	1.13	0.13403	0.00151	6.32489	0.07348	0.34208	0.00366	2,151	9	2022	10	1897	18
D1905-22	673	1817	1,290	1.41	0.11759	0.00124	3.38277	0.03725	0.20855	0.00220	1920	9	1,500	9	1,221	12
D1905-23	1,473	3,512	2,878	1.22	0.12659	0.00133	4.54329	0.04974	0.26017	0.00274	2051	9	1739	9	1,491	14
D1905-24	1723	4,822	3,150	1.53	0.12404	0.00131	4.47777	0.04921	0.26168	0.00276	2015	9	1727	9	1,498	14
D1905-25	1,276	11,731	3,472	3.38	0.11933	0.00134	4.48280	0.05179	0.27232	0.00289	1946	9	1728	10	1,553	15
D1911-1	572	1,084	1,006	1.08	0.12460	0.00142	6.32018	0.07413	0.36788	0.00395	2023	9	2021	10	2019	19
D1911-2	371	555	827	0.67	0.12823	0.00164	6.49443	0.08411	0.36733	0.00404	2074	10	2045	11	2017	19

(Continued on the following page)

10.3389/feart.2025.1592749

TABLE 1 (*Continued*) LA-ICP-MS zircon U-Pb dating data of mafic rocks from the Lieryu Formation.

Sample no.	Pb	Th	U	Th/U	Isotopic ratios						Ages(Ma)					
	ppm	ppm	ppm		$^{207}Pb/^{206}Pb$		$^{207}Pb/^{235}U$		$^{206}Pb/^{238}U$		$^{207}Pb/^{206}Pb$		$^{207}Pb/^{235}U$		$^{206}Pb/^{238}U$	
					Ratio	1σ	Ratio	1σ	Ratio	1σ	Ages	1σ	Ages	1σ	Ages	1σ
D1911-3	63	12	160	0.08	0.11110	0.00191	5.02307	0.08606	0.32791	0.00387	1817	15	1823	15	1828	19
D1911-4	177	31	444	0.07	0.11291	0.00136	5.10660	0.06295	0.32803	0.00354	1847	10	1837	10	1829	17
D1911-5	73	19	186	0.10	0.11070	0.00161	5.03549	0.07348	0.32991	0.00371	1811	12	1825	12	1838	18
D1911-6	84	36	409	0.09	0.11320	0.00157	5.11818	0.07148	0.32792	0.00365	1851	12	1839	12	1828	18
D1911-7	792	1,108	818	1.35	0.12360	0.00139	6.21194	0.07177	0.36450	0.00390	2009	9	2006	10	2003	18
D1911-8	43	20	210	0.10	0.11255	0.00207	5.10020	0.09326	0.32866	0.00397	1841	17	1836	16	1832	19
D1911-9	61	25	354	0.07	0.11253	0.00187	5.08592	0.08416	0.32780	0.00383	1841	15	1834	14	1828	19
D1911-10	468	459	1,108	0.41	0.12824	0.00139	6.53436	0.07290	0.36954	0.00392	2074	9	2051	10	2027	18
D1911-11	85	43	454	0.09	0.11291	0.00156	5.13940	0.07160	0.33013	0.00367	1847	12	1843	12	1839	18
D1911-12	108	27	289	0.09	0.11563	0.00157	5.19388	0.07140	0.32579	0.00361	1890	11	1852	12	1818	18
D1911-13	513	235	1,280	0.18	0.12660	0.00134	6.44375	0.07037	0.36916	0.00390	2051	9	2038	10	2025	18
D1911-14	73	33	385	0.09	0.11207	0.00165	5.11468	0.07550	0.33099	0.00373	1833	13	1839	13	1843	18
D1911-15	45	22	311	0.07	0.11381	0.00193	5.20784	0.08801	0.33187	0.00390	1861	15	1854	14	1847	19
D1911-16	55	30	338	0.09	0.11110	0.00190	5.08594	0.08660	0.33200	0.00391	1817	15	1834	14	1848	19
D1911-17	1951	1740	1,052	1.65	0.12956	0.00181	6.55776	0.09230	0.36711	0.00413	2092	11	2054	12	2016	19
D1911-18	184	41	453	0.09	0.11012	0.00143	5.05594	0.06677	0.33299	0.00365	1801	11	1829	11	1853	18
D1911-19	230	54	588	0.09	0.11019	0.00152	5.06371	0.07068	0.33329	0.00370	1803	12	1830	12	1854	18
D1911-20	31	13	249	0.05	0.11223	0.00226	5.17545	0.10337	0.33446	0.00418	1836	19	1849	17	1860	20
D1911-21	131	41	493	0.08	0.11501	0.00311	5.28803	0.14045	0.33348	0.00481	1880	28	1867	23	1855	23
D1911-22	157	21	395	0.05	0.11157	0.00166	5.14219	0.07692	0.33426	0.00378	1825	13	1843	13	1859	18

(Continued on the following page)

10.3389/feart.2025.1592749

TABLE 1 (*Continued*) LA-ICP-MS zircon U-Pb dating data of mafic rocks from the Lieryu Formation.

Sample no.	Pb	Th	U	Th/U	Isotopic ratios						Ages(Ma)					
	ppm	ppm	ppm		$^{207}Pb/^{206}Pb$		$^{207}Pb/^{235}U$		$^{206}Pb/^{238}U$		$^{207}Pb/^{206}Pb$		$^{207}Pb/^{235}U$		$^{206}Pb/^{238}U$	
					Ratio	1σ	Ratio	1σ	Ratio	1σ	Ages	1σ	Ages	1σ	Ages	1σ
D1911-23	65	22	364	0.06	0.11163	0.00168	5.15926	0.07804	0.33521	0.00381	1826	13	1846	13	1864	18
D1911-24	485	1,238	941	1.31	0.12761	0.00162	6.41757	0.08266	0.36475	0.00400	2065	10	2035	11	2005	19
D1914-1	481	480	962	0.50	0.13700	0.00199	7.22949	0.11504	0.38271	0.00501	2,190	13	2,140	14	2089	23
D1914-2	114	104	190	0.55	0.16477	0.00290	10.79461	0.20080	0.47515	0.00669	2,505	15	2,506	17	2,506	29
D1914-3	352	273	564	0.48	0.13718	0.00289	6.26158	0.13543	0.33104	0.00479	2,192	19	2013	19	1843	23
D1914-4	518	304	511	0.59	0.13702	0.00224	5.75449	0.10010	0.30458	0.00407	2,190	14	1940	15	1714	20
D1914-5	300	200	445	0.45	0.13693	0.00227	6.28356	0.11071	0.33282	0.00446	2,189	14	2016	15	1852	22
D1914-6	177	103	219	0.47	0.13696	0.00228	7.95994	0.14099	0.42151	0.00569	2,189	14	2,226	16	2,267	26
D1914-7	129	125	212	0.59	0.16503	0.00254	10.79194	0.17873	0.47428	0.00635	2,508	13	2,505	15	2,502	28
D1914-8	190	130	230	0.56	0.16518	0.00269	10.81260	0.18690	0.47475	0.00643	2,509	13	2,507	16	2,504	28
D1914-9	307	307	631	0.49	0.13729	0.00610	6.28438	0.27276	0.33197	0.00718	2,193	46	2016	38	1848	35
D1914-10	365	524	564	0.93	0.16474	0.00207	10.80702	0.15153	0.47576	0.00599	2,505	11	2,507	13	2,509	26
D1914-11	125	131	228	0.57	0.13706	0.00429	7.52443	0.23382	0.39816	0.00694	2,190	31	2,176	28	2,161	32
D1914-12	479	236	533	0.44	0.13718	0.00291	6.91263	0.15002	0.36547	0.00521	2,192	19	2,100	19	2008	25
D1914-13	361	32	1,002	0.03	0.11463	0.00148	5.26969	0.07513	0.33341	0.00414	1874	11	1864	12	1855	20
D1914-14	226	187	412	0.45	0.13697	0.00237	6.57604	0.11858	0.34819	0.00465	2,189	15	2056	16	1926	22
D1914-15	149	140	312	0.45	0.13703	0.00327	7.52304	0.18113	0.39816	0.00600	2,190	22	2,176	22	2,161	28
D1914-16	225	175	354	0.50	0.13715	0.00391	7.64817	0.21781	0.40444	0.00663	2,192	28	2,191	26	2,189	30
D1914-17	128	124	204	0.61	0.16447	0.00373	10.77160	0.24869	0.47497	0.00697	2,502	20	2,504	21	2,505	30
D1914-18	250	243	440	0.55	0.13703	0.00225	5.80887	0.09931	0.30743	0.00399	2,190	14	1948	15	1728	20

(Continued on the following page)

10.3389/feart.2025.1592749

TABLE 1 (*Continued*) LA-ICP-MS zircon U-Pb dating data of mafic rocks from the Lieryu Formation.

Sample no.	Pb	Th	U	Th/U	Isotopic ratios						Ages(Ma)					
	ppm	ppm	ppm		$^{207}Pb/^{206}Pb$		$^{207}Pb/^{235}U$		$^{206}Pb/^{238}U$		$^{207}Pb/^{206}Pb$		$^{207}Pb/^{235}U$		$^{206}Pb/^{238}U$	
					Ratio	1σ	Ratio	1σ	Ratio	1σ	Ages	1σ	Ages	1σ	Ages	1σ
D1914-19	415	158	365	0.43	0.13718	0.00245	6.90433	0.12795	0.36501	0.00477	2,192	16	2099	16	2006	23
D1914-20	251	245	523	0.47	0.13697	0.00508	7.09258	0.25938	0.37553	0.00711	2,189	38	2,123	33	2055	33
D1914-21	294	402	487	0.83	0.13704	0.00601	7.95568	0.34481	0.42102	0.00845	2,190	48	2,226	39	2,265	38
D1913-1	712	26	697	0.04	0.11443	0.00692	9.40326	0.58294	0.59592	0.01825	1871	28	2,378	57	3,013	74
D1913-2	261	3	730	0.00	0.11432	0.00251	5.81154	0.12897	0.35875	0.00482	1869	22	1948	19	1976	23
D1913-3	203	3	546	0.01	0.11436	0.00438	5.45646	0.20666	0.34600	0.00630	1870	22	1894	33	1915	30
D1913-4	505	7	429	0.02	0.11439	0.00397	5.44043	0.18728	0.34489	0.00590	1870	28	1891	30	1910	28
D1913-5	204	5	544	0.01	0.11445	0.00263	4.93731	0.11487	0.31283	0.00439	1871	23	1809	20	1755	22
D1913-6	292	28	764	0.04	0.11440	0.00302	4.98566	0.13202	0.31602	0.00469	1870	27	1817	22	1770	23
D1913-7	235	22	561	0.04	0.11437	0.00563	5.54855	0.26894	0.35178	0.00724	1870	28	1908	42	1943	35
D1913-8	335	4	925	0.00	0.11443	0.00195	5.06477	0.09026	0.32093	0.00411	1871	16	1830	15	1794	20
D1913-9	283	33	731	0.04	0.11439	0.00222	5.77593	0.11559	0.36614	0.00487	1870	18	1943	17	2011	23
D1913-10	357	33	953	0.03	0.11440	0.00295	4.74175	0.12232	0.30054	0.00443	1870	26	1775	22	1,694	22
D1913-11	490	19	540	0.03	0.11425	0.00401	4.92227	0.17094	0.31241	0.00536	1868	28	1806	29	1753	26
D1913-12	220	5	615	0.01	0.11435	0.00377	5.22547	0.17086	0.33136	0.00558	1870	25	1857	28	1845	27
D1913-13	370	28	1,041	0.03	0.11438	0.00190	4.74354	0.08243	0.30073	0.00385	1870	15	1775	15	1,695	19
D1913-14	233	21	646	0.03	0.11439	0.00161	5.31282	0.08061	0.33679	0.00417	1870	12	1871	13	1871	20
D1913-15	281	33	795	0.04	0.11445	0.00222	5.08784	0.10151	0.32238	0.00432	1871	18	1834	17	1801	21
D1913-16	572	22	838	0.03	0.11434	0.00183	5.73221	0.09675	0.36360	0.00465	1870	14	1936	15	1999	22
D1913-17	242	20	643	0.03	0.11434	0.00214	5.32781	0.10300	0.33794	0.00450	1870	17	1873	17	1877	22

(Continued on the following page)

TABLE 1 *(Continued)* LA-ICP-MS zircon U-Pb dating data of mafic rocks from the Lieryu Formation.

Sample no.	Pb	Th	U	Th/U	Isotopic ratios						Ages(Ma)					
	ppm	ppm	ppm		$^{207}Pb/^{206}Pb$		$^{207}Pb/^{235}U$		$^{206}Pb/^{238}U$		$^{207}Pb/^{206}Pb$		$^{207}Pb/^{235}U$		$^{206}Pb/^{238}U$	
					Ratio	1σ	Ratio	1σ	Ratio	1σ	Ages	1σ	Ages	1σ	Ages	1σ
D1913-18	181	3	500	0.01	0.11431	0.00190	5.51356	0.09619	0.34984	0.00452	1869	15	1903	15	1934	22
D1913-19	419	4	448	0.01	0.11431	0.00251	5.81154	0.12970	0.36875	0.00520	1869	21	1948	19	2024	24
D1913-20	342	20	886	0.02	0.11430	0.00661	5.99679	0.34047	0.38056	0.00960	1869	26	1975	49	2079	45
D1913-21	286	7	840	0.01	0.11442	0.00208	5.46120	0.10292	0.34623	0.00459	1871	17	1895	16	1917	22
D1913-22	330	31	937	0.03	0.11442	0.00166	5.15020	0.07973	0.32654	0.00410	1871	13	1844	13	1822	20
D1913-23	318	29	789	0.04	0.11440	0.00287	5.85216	0.14751	0.37112	0.00554	1870	25	1954	22	2035	26

length/width ratios of 2:1–4:1. The zoning cores with clear internal texture and white to gray unzoned rims are present in these grains. The ratios of Th/U range from 0.55 to 0.93, indicating a magmatic origin (Hoskin and Ireland, 2000; Belousova et al., 2002). Five analyses were obtained from five zircons, yielding a concordant $^{207}Pb/^{206}Pb$ age of 2,506 ± 6 Ma (n = 5, MSWD = 0.13). This age is interpreted as the captured zircons from the surrounding Archean rocks. The size of zircons from the other two groups is smaller with the diameter of 60–110 μm and length/width ratios of 1:1–2:1. The internal texture of zircons from the second group is clear with obvious oscillatory zoning. Combining with high Th/U ratios (0.43–0.83), indicating magmatic-derived zircon (Hoskin and Ireland, 2000; Belousova et al., 2002). Fifteen analyses yield an upper intercept $^{207}Pb/^{206}Pb$ age of 2,190 ± 13 Ma (n = 15, MSWD = 0.01), which is consistent with the $^{207}Pb/^{206}Pb$ weighted average age of 2,191 ± 30 Ma (n = 3, MSWD = 0.01) from 3 zircons on the concordant line (Figure 4a). This age is interpreted as the time of magmatic emplacement. The only one zircon (data 13) belongs to the third group. It exhibits white core, unzoned internal texture (Figure 3) and low ratio of Th/U (0.03), which indicates a metamorphic zircon (Hoskin and Ireland, 2000; Belousova et al., 2002). This zircon shows a concordant $^{207}Pb/^{206}Pb$ age of 1874 ± 11 Ma (Figure 4a) and is interpreted as a later metamorphism.

Zircons from sample D1913 are anhedral subrounded ranging in size from 30 to 65 μm with length/width ratios from 1:1–2:1. The white unzoned cores show unclear internal texture in these grains (Figure 3). With the Th/U ratios ranging from 0.01 to 0.09, these zircons were considered to be a metamorphic origin [43-46]. A total of twenty-three U-Pb isotopic analyses were conducted on zircons, yielding an upper intercept $^{207}Pb/^{206}Pb$ age of 1870 ± 2 Ma (n = 23, MSWD = 0.34), which is consistent with the weighted average $^{207}Pb/^{206}Pb$ age of 1870 ± 8 Ma (n = 23, MSWD = 0.01) (Figure 4C). This result is interpreted as the metamorphic age.

4.2 Major and trace element geochemistry

The average SiO_2 content of the amphibolite (D1902) is 50.47 wt%, while the other three mafic rocks show a lower average SiO_2 content (48.11–48.80 wt%). The Al_2O_3 content is moderate (12.63–14.14 wt%). The average total alkali content (K_2O + Na_2O) is moderate, ranging from 2.77 to 4.69 wt%. On the TAS diagram (Figure 5a), all the samples belong to the gabbro, and on the R1-R2 diagram (Figure 5b), they fall within the olivine-gabbro (olivine basalt) and gabbro norite area. The K_2O content of samples is variable, with average values from 0.81 wt% to 1.44 wt% respectively. On the SiO_2-K_2O diagram, the samples belong to the calc-alkaline to high-K calc-alkaline series (Figure 5c), and Ta/Yb vs. Ce/Yb ratios allow an allocation to the calc-alkaline series (Figure 5d). The average Fe_2O_3 content of the samples is 1.59–3.20 wt%, with a high average FeO content of 9.13–11.43 wt%, an average MgO content of 6.79–8.04 wt%, an average MnO content of 0.18–0.23 wt%. $Mg^{\#}$ ranges from 45.93 to 57.10, which is a little lower than that of primary basaltic rocks ($Mg^{\#}$ = 70, (Dupuy and Dostal, 1984). The average TiO_2 content of the amphibolite (D1905) is high (2.58 wt%) relatively, while the other three mafic rocks show a lower average TiO_2 content ranging from 1.02 wt% to 1.13 wt%. The amphibolite (D1905) exhibits a relatively low average CaO content (8.97 wt%)

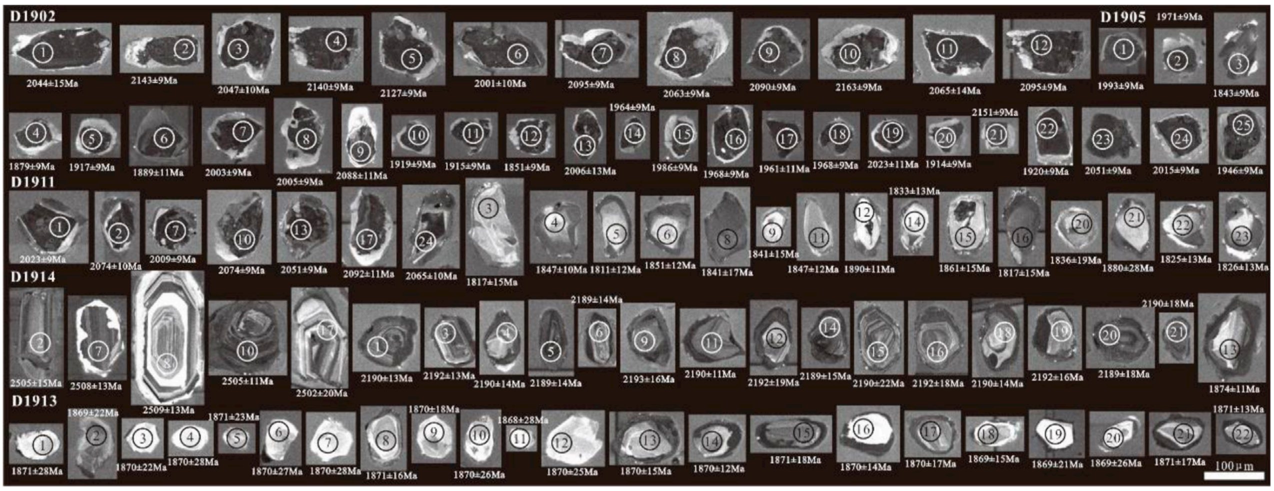

FIGURE 3
Cathodoluminescence (CL) images of the selected zircons from the mafic rocks in the Lieryu Formation. The circles on zircons represent analyzed spots.

and high P_2O_5 content (0.26 wt%), while the other three mafic rocks show a relatively high CaO content (10.02–10.42 wt%) and very low P_2O_5 content (0.07–0.12 wt%).

These mafic rocks show different characteristics of rare earth elements (REEs) and trace elements. The amphibolite (D1902) and the two gabbro (D1911, D1914) show low contents of total REEs, with average contents of 54.02 μg/g, 59.18 μg/g and 51.28 μg/g, respectively. They exhibit similar characteristics to enriched mid-ocean ridge basalt (E-MORB) on the chondrite-normalized rare earth element (REE) diagram, with a right-skewed smooth curve (Figure 6a), indicating an enrichment of light rare earth elements (LREEs) and a flat distribution pattern of heavy rare earth elements (HREEs). The differentiation between LREEs and HREEs is low, with an average $(La/Yb)_N$ value of 2.08–4.43 and a slight positive europium anomaly (Eu/Eu^*= 1.03–1.21) (Figure 6a). The other amphibolite (D1905) shows same trend with E-MORB, but with a high average REEs contents, which is 137.70 μg/g (Sun and McDonough, 1989). On the chondrite-normalized REE diagram, the samples show a right-skewed curve (Figure 6a), indicating a slight differentiation between them, with average $(La/Yb)_N$ values of 3.31. This amphibolite shows a slight negative europium anomaly (Eu/Eu^*= 0.92–0.97) (Figure 6a).

In the primitive mantle-normalized trace element spider diagram, these mafic rocks demonstrate different characteristics. The amphibolite (D1902) exhibits significantly varying incompatible elements, with an enrichment of large ion lithophile elements (LILEs) (Rb, K, etc.), depletion of high field strength elements (HFSEs) (Nb, Ta, Zr, Ti, etc.), and slight negative anomalies of Sr and P, as well as positive anomalies of Th and U (Figure 6b). The average contents of Cr, Co and Ni are 52.0 μg/g, 41.3 μg/g and 19.3 μg/g respectively. The other amphibolite (D1905) shows relatively high overall elemental content, with an enrichment of LILEs (Rb, Ba, K, etc.), and strong negative anomalies of Sr and P, as well as slight positive anomalies of U, Zr and Hf (Figure 6b). The average contents of Cr, Co and Ni are 132 μg/g, 33.1 μg/g and 49.1 μg/g respectively, which is slightly higher than N-MORB. The two gabbro (D1911, D1914) have a roughly same pattern, with an enrichment of LILEs (Rb, Ba, K, etc.), depletion of HFSEs (Th, Nb, Ta, Ce, Zr, Ti, etc.), and negative anomalies of P. The gabbro shows positive anomalies of Sr, with the D1911 being a slight positive anomaly and the D1914 being a strong positive anomaly (Figure 6b). They have different contents of Cr, Co and Ni, with the contents of Cr (with average contents of 22.0 μg/g and 189.0 μg/g), Co (with average contents of 43.5 μg/g and 46.7 μg/g), and Ni (with average contents of 38.0 μg/g and 68.4 μg/g).

5 Discussion

5.1 The limitations of geochronology on the relationships between the formations of the Liaohe group

Since the initial investigations of the Liaohe Group in the late 1930s, this Precambrian sequence has been conventionally interpreted as an ordered stratigraphic column comprising, from bottom to top: the Langzishan, Lieryu, Gaojiayu, Dashiqiao, and Gaixian Formations (Liaoning Bureau of Geology and Mineral Resources, 2017). These units were historically perceived to exhibit an orderly stratigraphic succession from bottom to top in the typical sections of the Liaohe Group. However, recent investigations have challenged this traditional stratigraphic framework. Based on lithological assemblages and zircon geochronological data, Li *et al.* (2014) proposed that the Langzishan Formation correlates temporally with the Gaixian Formation of the southern Liaohe Group, suggesting its uppermost position within the sequence. The age of the amphibolite obtained from the Langzishan Formation also indicates that the Langzishan Formation is no longer suitable to be placed beneath the Lieryu Formation (Chen et al., 2018). The preservation of original stratigraphic relationships remains questionable given the complex Paleoproterozoic tectonic evolution that affected the region (Zhao et al., 2012; Liu et al., 2015). Field

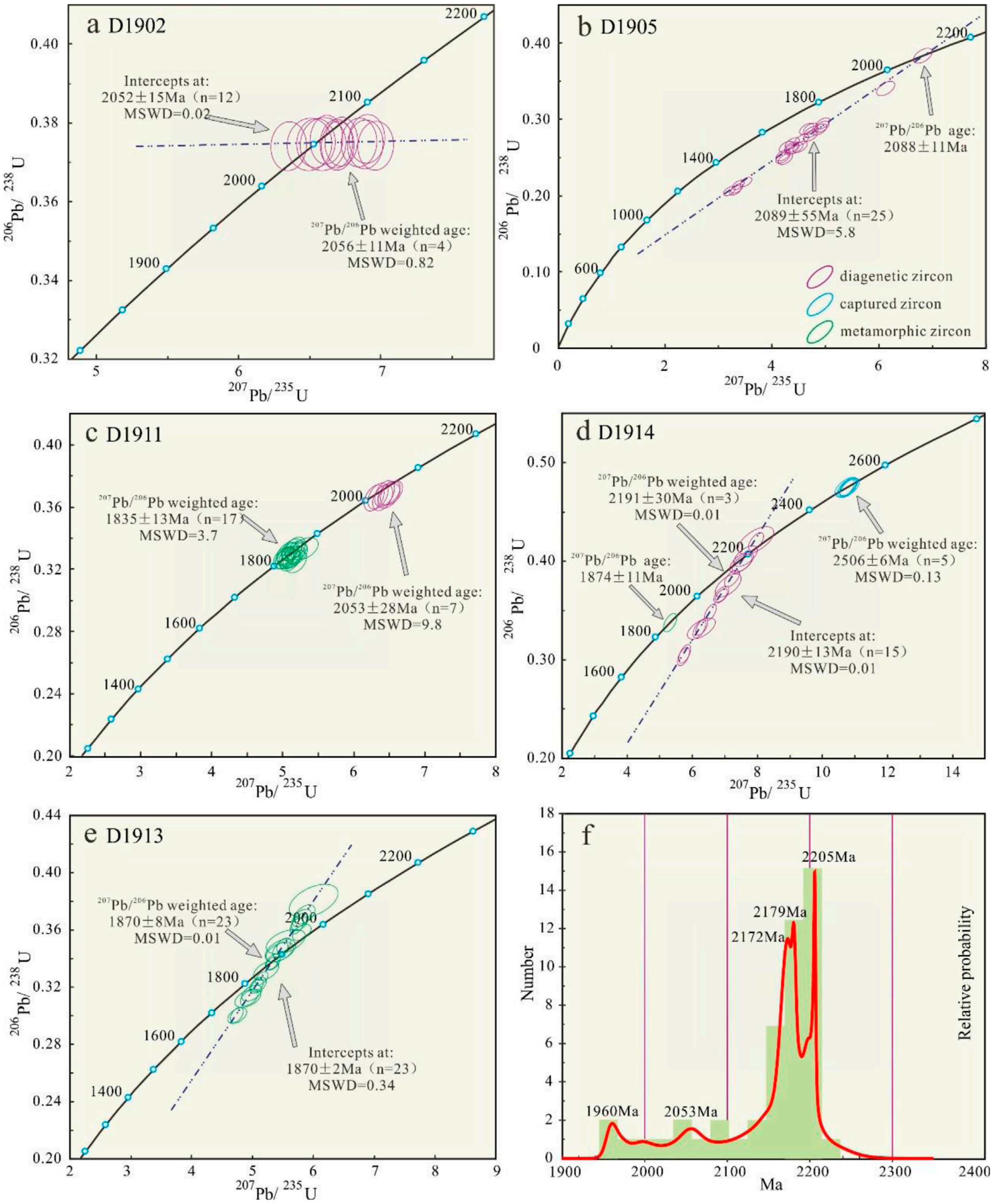

FIGURE 4
Concordia diagrams for zircons analysed from mafic rocks **(a–e)** and summary of geochronological data of volcanic rocks **(f)** in the Lieryu Formation.

investigations by Chen et al. (2017a) along the “typical sections” revealed that most metamorphic rocks from the Liaohe Group exhibit characteristics of contact and dynamic metamorphism, with various lithologies occurring in interlayered patterns. Crucially, the boundaries between formations predominantly manifest as ductile shear zones rather than conformable contacts (Chen et al., 2017a). Furthermore, the coeval presence of low-grade and high-grade metamorphic sequences within both the Gaojiayu and Gaixian Formations (Liu et al., 2015) provides additional evidence against the preservation of an intact stratigraphic succession. These findings collectively suggest that the Liaohe Group is no longer orderly strata, but represent a structural rock assemblage resulting from polyphase metamorphic and deformation events.

Chronostratigraphic studies reveal significant variations in the formation ages of different lithostratigraphic units within the Liaohe Group (Table 2). The mafic volcanic rocks from the Langzishan Formation yield a crystallization age of 1952 ± 38 Ma (Chen et al., 2018), while detrital zircon analyses constrain their

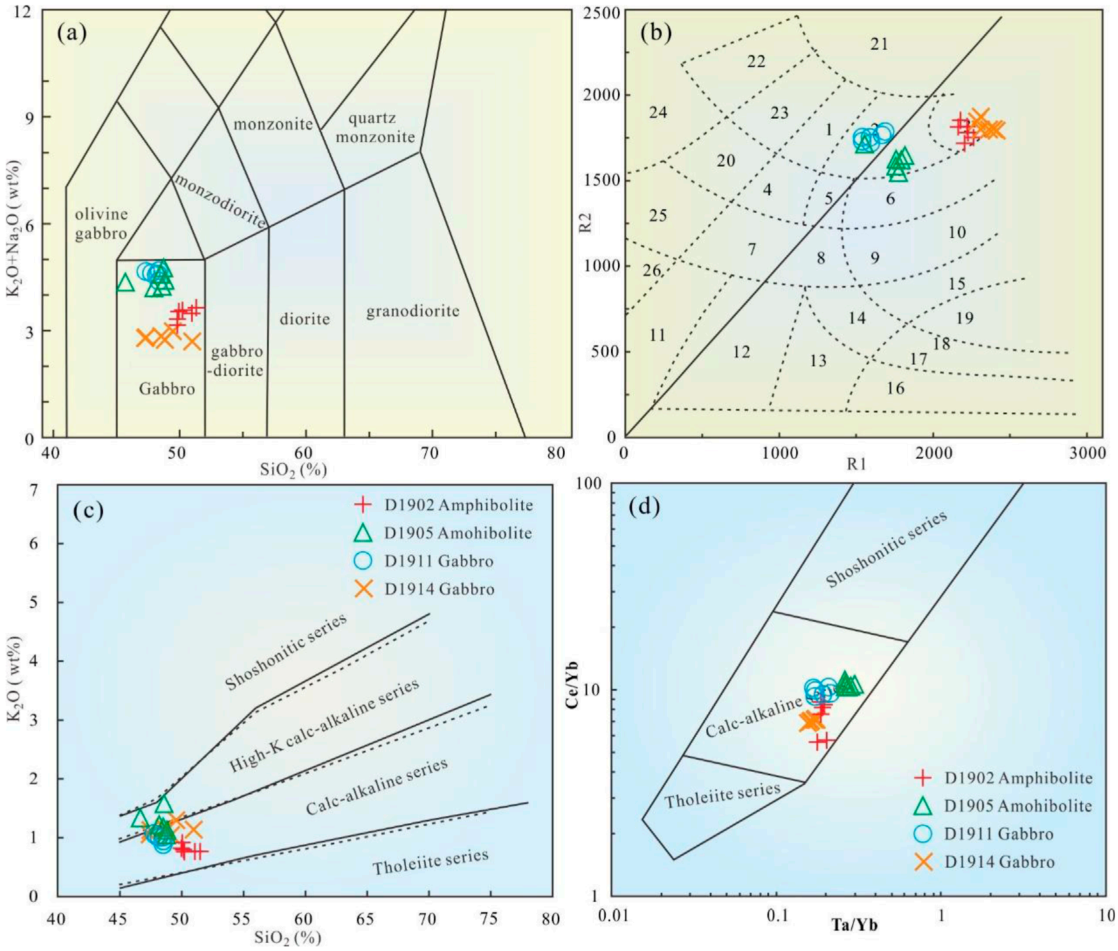

FIGURE 5
SiO_2 vs. total alkali (Na_2O + K_2O) **(a)**, after (Middlemost, 1994), R1 vs. R2 **(b)**, after (De la Roche et al., 1980), SiO_2-K_2O **(c)**, after (Peccerillo and Taylor, 1976) and Ta/Yb vs. Ce/Yb **(d)**, after (Pearce, 1982) diagrams for mafic rocks from Lieryu Formation. **(b)** 1—alkaline gabbro (alkaline basalt); 2—olivine gabbro (olivine basalt); 3—gabbro norite (tholeiite); 4—syenite gabbro (trachyte basalt); 5—monzonite gabbro (andesite coarse basalt); 6—gabbro (basalt); 7—trachyandesite (syenite); 8—monzonite (andesite); 9—monzodiorite (trachyte); 10—diorite (andesite); 11—nepheline syenite (trachyte phonolite); 12—syenite (trachyte); 13—quartz syenite (quartz trachyte); 14—quartz monzonite (quartz andesite); 15—tonalite (dacite); 16—alkaline granite (alkaline rhyolite); 17—syenogranite (rhyolite); 18—monzogranite (dacite rhyolite); 19—granodiorite (rhyolite dacite); 20—essenite-aegirine gabbro; 21—peridotite (picrite); 22—nepheline (picrite nepheline); 23—qilieyan (basanite); 24—neonite (nepheline); 25—essenite; 26—nepheline syenite (phonolite).

depositional age to post-2078 Ma (Luo et al., 2004). In contrast, the Lieryu Formation exhibits the most extensive volcanic exposures, though previous investigations predominantly focused on felsic rocks. These studies reveal a long formation time of the felsic rocks ranging from 2,229 to 1959 Ma (Li and Chen, 2014; Li et al., 2015a; Li et al., 2015b; Li et al., 2019a; Chen et al., 2016; 2017a; Meng et al., 2017; Bi et al., 2018b; Liu et al., 2018; Xu et al., 2019). Amphibolite geochronology from this formation constrains its mafic magmatism to 2,159–1995 Ma (Chen et al., 2020a; Gao et al., 2017; Meng et al., 2017). The new U-Pb zircon ages of 2052 ± 15 Ma, 2089 ± 55 Ma, 2053 ± 28 Ma, and 2,190 ± 13 Ma from mafic rocks in this study refine the geochronological framework of Lieryu mafic magmatism to 2,190–1995 Ma. Therefore, the age of the Lieryu Formation ranges from 2,229 to 1959 Ma under the limitation of the geochronological results of felsic volcanic rocks and mafic rocks. The volcanic rocks from the Gaojiayu Formation exhibit an age range of 2,184–1928 Ma (Chen et al., 2017b; Bi et al., 2018a; Dong et al., 2019), whereas the Dashiqiao Formation volcanics were emplaced between 2,171 and 2054 Ma (Chen et al., 2017b; Xu et al., 2018a; b; Dong et al., 2019). From the above, the overlapping age among these formations (2078–1952 Ma for Langzishan, 2,229–1959 Ma for Lieryu, 2,184–1928 Ma for Gaojiayu, and 2054–2,171 Ma for Dashiqiao) did not show a continuous sedimentary strata but a disordered relationships, which reveals that the relationship between the various formation of the Liaohe Group is not a conformable stratigraphic succession. Combined with a set of boron-associated mélange assemblage (peridotite, gabbro, tourmaline granulite, and plagiogranite) distinguished from the Lieryu Formation, it also indicates that the Liaohe Group is not an ordered stratum.

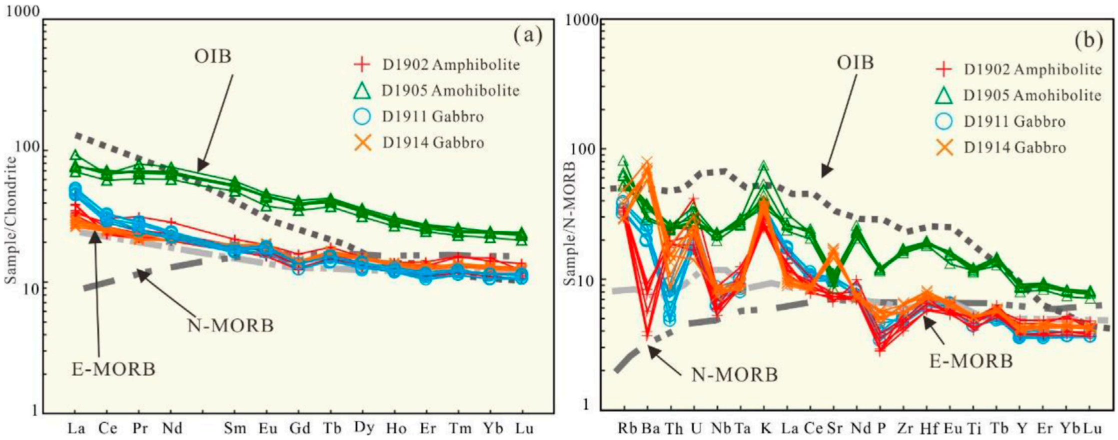

FIGURE 6
Chondrite-normalized rare earth element patterns **(a)** and primitive mantle-normalized trace element spider diagram **(b)** for the mafic rocks from Lieryu Formation. (The values of chondrite and primitive mantle are from (Sun and McDonough, 1989).

5.2 Source and genesis of the mafic rocks

The mafic rocks of the Lieryu Formation in Liaodong have undergone low- to medium-grade metamorphism, such as epidotization, and chloritization. Under changing conditions, strong active elements tend to migrate, whereas REEs and HFSEs remain relatively stable. Consequently, these elements can be utilized to reconstruct and investigate the magmatic series, genesis, and source characteristics of these mafic rocks (Rollinson, 1993; Kerrich et al., 1999).

Typically, mafic rocks originate from either the lithospheric mantle or the asthenospheric mantle, with partial melting of lithospheric mantle rocks resulting in negative europium (Eu) anomalies (Sklyarov et al., 2003). These mafic rocks exhibit enrichment in LREEs and LILEs, along with depletion of HREEs and HFSEs such as Nb, Ta, Ti, Zr Ce and Th. They also show either positive europium anomaly ($Eu/Eu^* = 1.03–1.21$) or a slight negative europium anomaly ($Eu/Eu^* = 0.92–0.97$). In the pattern of the REEs and trace elements, the amphibolite (D1902) and two gabbro (D1911, D1914) are similar to E-MORB suggesting a source from the asthenospheric mantle, while the other amphibolite (D1905) resembles OIB (Figure 7a) indicating a complicated mantle source (Sklyarov et al., 2003). On the Nb/Th-Zr/Nb figure,the amphibolite (1905) and the gabbro (1911) are positioned near the primitive mantle (PM) (Fugure 7a), the amphibolite (1902) is close to the enrichment mantle (EM), the gabbro (1914) lies between the PM and EM (Fugure 7a). In the La/Yb-Th/Ta diagram, these mafic rocks distribute in the middle of PM and EM (Figure 7b). These features suggest that these mafic rocks are originated from the transitional mantle.

The nature of the original magma in the source can be studied by content and ratio of trace elements, due to their similar distribution coefficients and is difficult to fractionate during partial melting or fractional crystallization (McKenzie and O'Nions, 1991). Three mafic rocks (D1902, D1905, D1914) show similar patterns of flat REEs, with a lower LREE/HREE ratio (2.80–3.66, 3.58–3.73 and 2.86–2.96 respectively), indicating that there may be no residual garnet in the source (Figures 7c,d). They are located at the Amphibole-bearing spinel lherzolite melting curve on the La/Yb-Yb diagram (Figure 7c), indicating the presence of residual amphibole and spinel in the magma source. But there is difference on the melting degree, with 3%–4% melting degree of the amphibolite (D1905) and 10%–20% melting degree of the amphibolite (D1902) and gabbro (D1914) (Figure 7c). The other gabbro (D1911) shows a pattern of relatively enrichment in LREEs, flat HREEs, high ratios of LREE/HREE (3.94–4.19), which indicates that garnet may be the residual mineral in the source. On the La/Yb-Yb diagram, the gabbro is located at the Garnet spinel lherzolite melting curve with the garnet to spinel ratio being 50:50 (Figure 7c), indicating the presence of residual garnet and spinel in the magma source.

In contrast to the partial melting of spinel lherzolite, the partial melting of various proportions of clinopyroxene and garnet exhibits distinct characteristics in the La/Sm and Sm/Yb ratios. Notably, the Sm/Yb ratio remains unaffected by the decrease in La/Sm (Aldanmaz et al., 2000). These mafic rocks show the similar characteristics on the $(La/Sm)_N$-$(Sm/Yb)_N$ diagram (Figure 7d). Consistent with the above conclusion, there is no garnet in the magma source of the three mafic rocks (D1902, D1905, D1914). They are the melting product of amphibole-bearing spinel lherzolite, showing different partial melting degrees of about 1%–2%, 3%–4%, and around 10%, respectively (Figure 7d). The other gabbro is product of partial melting of garnet–spinel lherzolite with a ratio of clinopyroxene to garnet of 6:1 in the 5%–10% melting degree (Figure 7d; Jourdan et al., 2007). The amphibolite (D1905) shows negative Sr anomaly (Figure 6b), indicating the possible residual plagioclase in the source. And the positive Sr anomaly of the gabbro (D1914) indicates no residual plagioclase in its magma source (Figure 6b).

These mafic rocks exhibit similar characteristics to of island arc basalt (IAB): enrichments in LREEs and LILEs such as Rb, Ba, and K, as well as depletions in HFSEs such as Nb, Ta, Zr, Hf, Ti, and P. It may be related to the subduction fluids or the involvement of island arc components, indicating that metasomatic processes occurred in the source (Sun and Nesbitt, 1978). Thus, is the metasomatism caused by melts or fluids? When the metasomatism occurred in the

TABLE 2 Geochronological data of different formation from the Liaohe Group in the Liao-Ji Belt.

NO.	Sample	Lithology	Age	Formation	Location	Analysis methord	Reference
1	SJZ07-5	Amphibolite	2054-2061 Ma	Dashiqiao Formation	Sanjiazi Town	Zircon (LA-ICPMS)	Xu et al. (2018a), Xu et al. (2018b)
2	16KD55-1-1	Amphibolite	2063 ± 23 Ma	Dashiqiao Formation	Sanjiazi Town	Zircon (LA-ICPMS)	Xu et al. (2018a), Xu et al. (2018b)
3	D2066-11	Amphibolite	2083 ± 13 Ma	Dashiqiao Formation	Helan Town	Zircon (LA-ICPMS)	Xu et al. (2018a), Xu et al. (2018b)
4	SJZ11-1	Amphibolite	2,119 ± 19 Ma	Dashiqiao Formation	Sanjiazi Town	Zircon (LA-ICPMS)	Xu et al. (2018a), Xu et al. (2018b)
5	16XY014	Meta-rhyolite	2,170 ± 11 Ma	Dashiqiao Formation	Xiuyan City	Zircon (LA-ICPMS)	Dong et al. (2019)
6	16XY003	Meta-rhyolite	2,170 ± 29 Ma	Dashiqiao Formation	Xiuyan City	Zircon (LA-ICPMS)	Dong et al. (2019)
7	14GW580	Felsic breccia tuff	2,171 ± 11 Ma	Dashiqiao Formation	Huayansi Town	Zircon (LA-ICPMS)	Chen et al. (2017b)
8	HLY-3	Basalt	1928 Ma	Gaojiayu Formation	Helan Town	Zircon (LA-ICPMS)	Chen et al. (2020a)
9	D15054	Amphibolite	1985 Ma	Gaojiayu Formation	Helan Town	Zircon (LA-ICPMS)	Chen et al. (2020b)
10	D1423-1	Amphibolite	2079 Ma	Gaojiayu Formation		Zircon (LA-ICPMS)	Chen et al. (2020b)
11	TWD15002	Rhyolite	2,127 ± 25 Ma	Gaojiayu Formation	Tianshui Town	Zircon (LA-ICPMS)	Bi et al. (2018a)
12	TWD15026-2	Meta-rhyolite	2,137 ± 9 Ma	Gaojiayu Formation	Xiuyan City	Zircon (LA-ICPMS)	Dong et al. (2019)
13	D1488-1	Amphibolite	2145 Ma	Gaojiayu Formation		Zircon (LA-ICPMS)	Chen et al. (2020b)
14	TWD15026-1	Meta-rhyolite	2,166 ± 17 Ma	Gaojiayu Formation	Xiuyan City	Zircon (LA-ICPMS)	Dong et al. (2019)
15	TWD15001	Rhyolite	2,179 ± 20 Ma	Gaojiayu Formation	Tianshui Town	Zircon (LA-ICPMS)	Bi et al. (2018a)
16	D15015	Rhyolite	2179 Ma	Gaojiayu Formation	Helan Town	Zircon (LA-ICPMS)	Chen et al. (2020b)
17	D1442-1	Meta-felsic breccia-bearing tuff	2,180 ± 12 Ma	Gaojiayu Formation	Huayansi Town	Zircon (LA-ICPMS)	Chen et al. (2017a)
18	TWD15056	Rhyolite	2,184 ± 11 Ma	Gaojiayu Formation	Tianshui Town	Zircon (LA-ICPMS)	Bi et al.(2018a)
19	D14114-1b	Rhyolite	1959 ± 6 Ma	Lieryu Formation	Huayansi Town	Zircon (LA-ICPMS)	Chen et al. (2017a)
20	D14109-2	Rhyolite	1969 ± 9 Ma	Lieryu Formation	Lianshanguan Town	Zircon (LA-ICPMS)	Chen et al. (2017a)
21	D1002-B1	Amphibolite	1995 ± 13 Ma	Lieryu Formation	Huanghuadianzi Town	LA-ICPMS	Gao et al. (2017)
22	D019	Amphibolite	2024 ± 33 Ma	Lieryu Formation	124°58′14.9″,40°47′22.5″	Zircon (LA-ICPMS)	Chen et al. (2020a)
23	D014	Amphibolite	2053 Ma	Lieryu Formation	124°55′53″,40°39′13″	Zircon (LA-ICPMS)	Chen et al. (2020a)

(Continued on the following page)

TABLE 2 (*Continued*) Geochronological data of different formation from the Liaohe Group in the Liao-Ji Belt.

NO.	Sample	Lithology	Age	Formation	Location	Analysis methord	Reference
24	D14112-1	Rhyolite	2,100 ± 27 Ma	Lieryu Formation	Lianshanguan Town	Zircon (LA-ICPMS)	Chen et al. (2020a)
25	D018	Amphibolite	2,130 ± 19 Ma	Lieryu Formation	124°58′43.8″,40°47′12.8″	Zircon (LA-ICPMS)	Chen et al. (2020a)
26	JZ28-2	Biotite fine-grained gneiss	2,135 ± 46 Ma	Lieryu Formation	Fengcheng City	LA-ICPMS	Meng et al. (2017)
27	D4034-B1	Amphibolite	2,150 ± 21 Ma	Lieryu Formation	Huanghuadianzi Town	LA-ICPMS	Gao et al. (2017)
28	TWD15013	Rhyolite	2,153 ± 11 Ma	Lieryu Formation	Liaoyang City	Zircon (LA-ICPMS)	Bi et al. (2018b)
29	LZ19-1	Fine-grained gneiss	2,158 ± 22 Ma	Lieryu Formation	Zhoujia Town	Zircon (LA-ICPMS)	Li and Chen, (2014)
30	DZ40-2	Amphibolite	2,159 ± 28 Ma	Lieryu Formation	Fengcheng City	LA-ICPMS	Meng et al. (2017)
31	16SMT03-1	Felsic tuff	2,168 ± 6 Ma	Lieryu Formation	Helan Town	Zircon (SHRIMP)	Xu et al. (2019)
32	D5049-1.5	Felsic tuff	2,170 ± 7 Ma	Lieryu Formation	Helan Town	Zircon (SHRIMP)	Xu et al. (2019)
33	N02	Tourmalinite	2,171 ± 6 Ma	Lieryu Formation	Dashiqiao City	SHRIMP	Zhang et al. (2010)
34	N14	Tourmalinite	2,171 ± 9 Ma	Lieryu Formation	Dashiqiao City	SHRIMP	Zhang et al. (2010)
35	LZ04-1	Fine-grained gneiss	2,172 ± 8 Ma	Lieryu Formation	Zhoujia Town	Zircon (LA-ICPMS)	Li and Chen, (2014)
36	D2092-1.2	Felsic tuff	2,174 ± 8 Ma	Lieryu Formation	Helan Town	Zircon (SHRIMP)	Xu et al. (2019)
37	16SMT02-1	Felsic tuff	2,174 ± 8 Ma	Lieryu Formation	Helan Town	Zircon (SHRIMP)	Xu et al. (2019)
38	N13	Tourmalinite	2,175 ± 5 Ma	Lieryu Formation	Dashiqiao City	SHRIMP	Zhang et al. (2010)
39	JL29-1	Biotite-plagioclase gneiss	2,176 ± 22 Ma	Lieryu Formation	Fengcheng City	LA-ICPMS	Meng et al. (2017)
40	LD0106-1	Biotite gneiss	2,179 ± 8 Ma	Lieryu Formation	Dashiqiao City	SHRIMP	Wan et al. (2005)
41	DHL-N2	Tourmaline-bearing felsic gneiss	2,181 ± 2 Ma	Lieryu Formation	N40°34′37″, E123°24′00″	LA-ICPMS	Liu et al. (2018)
42	HX35	Meta-andesite	2,182 ± 6 Ma	Lieryu Formation	N40°21′25″, E122°55′27″	LA-ICPMS	Chen et al. (2016)
43	14GW585	Rhyolite	2,185 ± 16 Ma	Lieryu Formation	Huayansi Town	Zircon (LA-ICPMS)	Chen et al. (2017a)
44	D1444-2	Rhyolite	2,191 ± 46 Ma	Lieryu Formation	Huayansi Town	Zircon (LA-ICPMS)	Chen et al. (2017a)
45	HX-35	Meta-andesite	2,195 ± 6 Ma	Lieryu Formation	N40°21′25″, E122°55′27″	LA-ICPMS	Li et al. (2018)

(Continued on the following page)

TABLE 2 (*Continued*) Geochronological data of different formation from the Liaohe Group in the Liao-Ji Belt.

NO.	Sample	Lithology	Age	Formation	Location	Analysis methord	Reference
46	HX-33	Meta-andesite	2,199 ± 6 Ma	Lieryu Formation	N40°21′25″, E122°55′27″	LA-ICPMS	Li et al. (2018)
47	LZ3	Meta-rhyolite	2,201 ± 5 Ma	Lieryu Formation	Jianyi Town	Zircon (LA-ICPMS)	Li et al. (2015a), Li et al. (2015b)
48	LZ02-1	Fine-grained gneiss	2,204 ± 11 Ma	Lieryu Formation	Zhoujia Town	Zircon (LA-ICPMS)	Li and Chen, (2014)
49	HX-38	Meta-rhyolite	2,205 ± 2 Ma	Lieryu Formation	N40°21′25″, E122°55′27″	LA-ICPMS	Li et al. (2018)
50	HX-37	Meta-rhyolite	2,206 ± 1 Ma	Lieryu Formation	N40°21′25″, E122°55′27″	LA-ICPMS	Li et al. (2018)
51	JL40-2	Biotite fine-grained gneiss	2,209 ± 21 Ma	Lieryu Formation	Fengcheng City	LA-ICPMS	Meng et al. (2017)
52	HX33	Meta-andesite	2,229 ± 22 Ma	Lieryu Formation	N40°21′25″, E122°55′27″	LA-ICPMS	Chen et al. (2016)
53	D1902	Amphibolite	2056 ± 11 Ma	Lieryu Formation	Jianyi Town	Zircon (LA-ICPMS)	This study
54	D1905	Amphibolite	2089 ± 55 Ma	Lieryu Formation	Gushan Town	Zircon (LA-ICPMS)	This study
55	D1911	Gabbro	2053 ± 28 Ma	Lieryu Formation	Nuanhe Boron Mine	Zircon (LA-ICPMS)	This study
56	D1914	Gabbro	2,190 ± 13 Ma	Lieryu Formation	Pianling Town	Zircon (LA-ICPMS)	This study
57	D021	Amphibolite	1952 ± 38 Ma	Langzishan Formation	Zhujiagou villiage	Zircon (LA-ICPMS)	Chen et al. (2018)
58	02L098-1	Mica Schist	2078 ± 43 Ma	Langzishan Formation	N40°45′28″, E122°44′33″	Zircon (LA-ICPMS)	Luo et al. (2004)

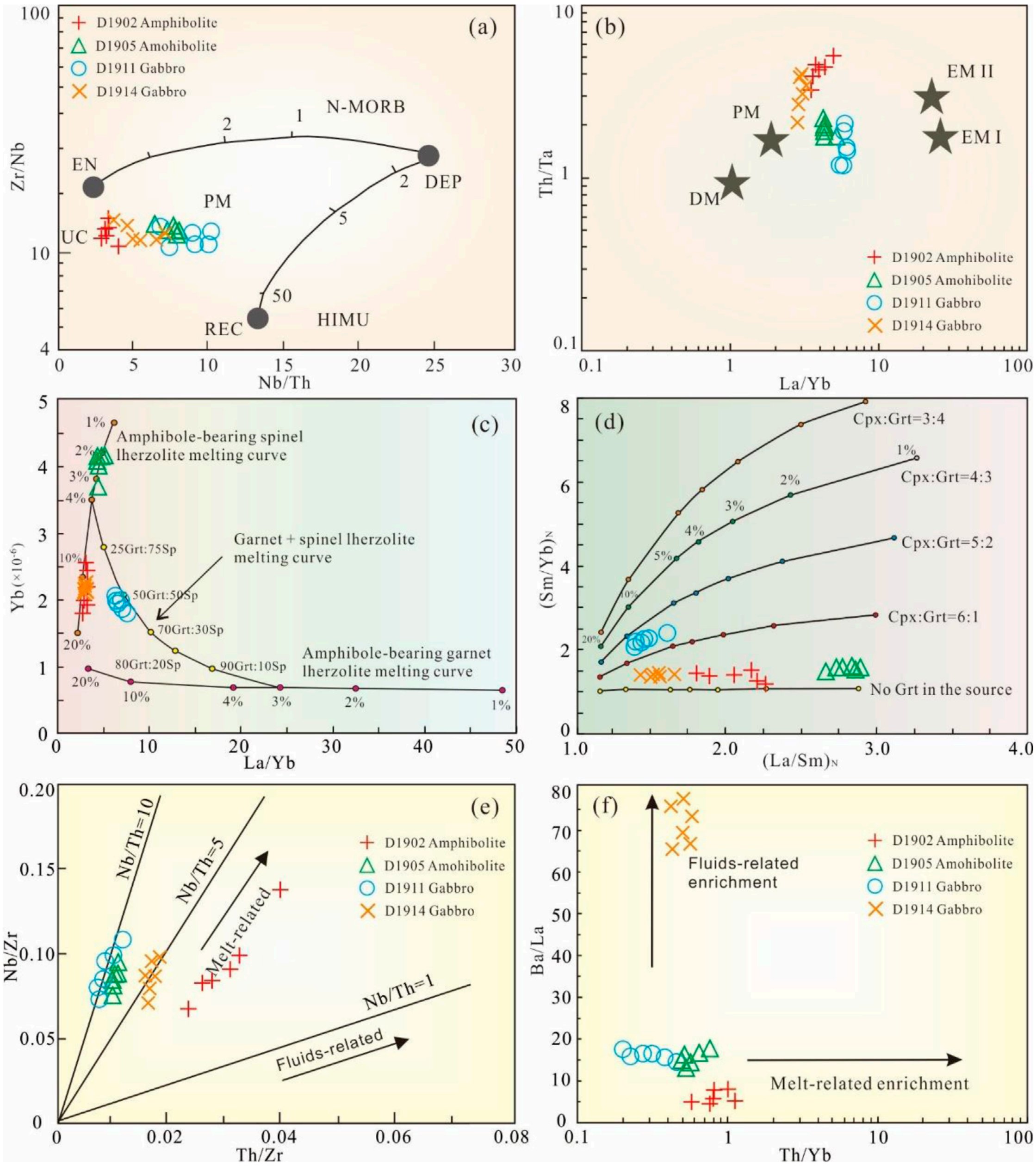

FIGURE 7
Source characteristics of the mafic rocks from the Lieryu Formation **(a)**. After Condie et al., 2002, DEP-depleted mantle, EN-enriched mantle, N-MORB-normal mid-ocean ridge basalt, PM-primitive mantle, REC-recycled plate, UC-upper crust; **(b)** After Zhang et al., 2012; DM-depleted mantle, PM-primitive mantle, EM I-enriched mantle I, EM II- enriched mantle II; **(c,d)** After McKenzie and O'Nions, 1991, Grt- garnet, SP-spine, Cpx-clinopyroxene; **(e,f)** After Woodhead et al., 2001.

source is caused by melts, the magma generally exhibits high Na_2O, P_2O_5, and TiO_2 contents (Sajona et al.,2000), or obvious negative Ce anomaly (Plank and Langmuir, 1998). The D1902 (amphibolite), D1905 (amphibolite) and D1911 (gabbro) exhibit high Na_2O content and negative Ce anomalies (average Ce/Ce*= 0.87, 0.91 and 0.87 respectively), indicating a melt related metasomatism in the source, which is consistent with the trends shown in the Th/Zr-Nb/Zr and Th/Yb-Ba/La diagram (Figures 7e, f). The D1914 (gabbro) exhibits a low Na_2O, P_2O_5, and TiO_2 contents, with no Ce anomaly (average Ce/Ce*= 1.00), indicating the source has undergone fluid metasomatism, which is consistent with the trends shown in the Th/Yb-Ba/La diagram (Figure 7f). But, the characteristics of Th/Zr and Nb/Zr ratio indicate that it also has undergone melt metasomatism (Figure 7e). The higher Cr, Co and Ni content than N-MORB in D1914 also suggests a melt related metasomatism in the source. So the D1914 (gabbro) has undergone dual metasomatism of fluid and melt, while the others mafic rocks are mainly influenced by melt metasomatism.

Generally, during the process of ascent and emplacement, mantle-derived magma may experience assimilation and

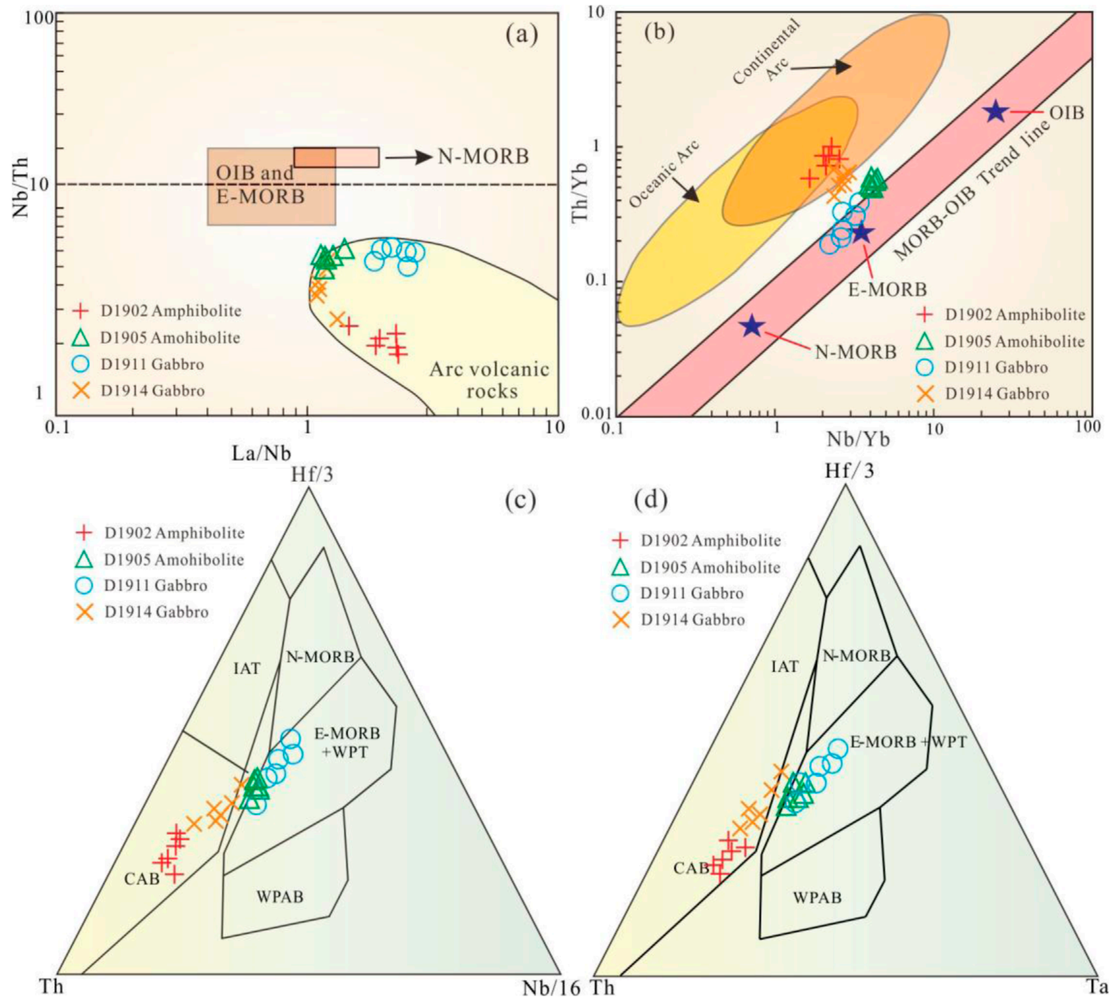

FIGURE 8
Identification diagram of tectonic setting for the mafic rocks from the Lieryu Formation. **(a)** La/Nb versus Nb/Th diagram (Zhang et al., 2012); **(b)** Nb/Yb versus Th/Yb diagram (after Pearce, 1996); **(c)** Hf/3 versus Th versus Nb/16; **(d)** Hf/3 versus Th versus Th/Yb diagram (after Pearce, 1982).

contamination with crustal materials. Geochemical data for these mafic rocks indicate moderate to high levels of potassium and alkali content (Figure 5c), low Mg# values (Mg# = 45.93–57.61), enrichment in LILEs such as Rb, Ba, and K, and depletion in HFSEs like Th, Nb, Ta, and Zr. These characteristics suggest that the magma has likely been contaminated by crustal materials (Wu et al., 2007). These mafic rocks have a lower Nb/Ta ratios (averaging 11.04, 14.04, 14.00, and 16.03) and Zr/Hf ratios (averaging 26.19, 31.80, 28.19, and 28.64) than the continental crust in eastern China (Nb/Ta = 15.38, Zr/Hf = 35.56, according to Chi and Yan, 2007), as well as the mid-ocean ridge basalts (MORB) and the primitive mantle (Nb/Ta = 17.7, Zr/Hf = 36.1, Sun and McDonough, 1989). These differences suggest that crustal contamination has influenced the mafic magmas. The La/Sm ratio is frequently used to assess the degree of crustal contamination (Zhang et al., 2019). A higher La/Sm ratio generally signifies a stronger influence of crustal components, whereas a lower ratio may indicate a more pristine mantle source (Zhang et al., 2019). The average La/Sm ratios of these mafic rocks are 16.37, 15.92, 18.24, and 13.88, respectively, reflecting the assimilation and contamination of continental crustal composition during magma ascent. The contamination level is highest in D1911 (gabbro), followed by D1902 (amphibolite) and D1905 (amphibolite), with the lowest contamination found in D1914 (gabbro).

In conclusion, the Paleoproterozoic mafic rocks originated from a transitional mantle source, of which the D1902 (amphibolite), D1905 (amphibolite) and D1911 (gabbro) are mainly influenced by melt metasomatism, while the D1914 (gabbro) has undergone dual metasomatism of fluid and melt in the source. The D1902 (amphibolite), D1905 (amphibolite) and D1914 (gabbro) are product of 2%–3% or 10%–20% partial melting of amphibole-bearing spinel lherzolite, leading to residual hornblende and spinel in the source. The D1911 (gabbro) is product of 3%–4% partial melting of garnet–spinel lherzolite with the 50:50 ratios of garnet and spinel and 6:1 ratio of clinopyroxene to garnet, resulting in garnet and spinel in the source. During the ascent and emplacement, assimilation and contamination occurred between mafic magmas and continental crustal materials.

5.3 Tectonic significance of mafic rocks

TiO_2 contents vary in mafic rocks formed in different tectonic environments (Wilson, 1989). Ocean island basalt (OIB) typically has the highest TiO_2 content, reaching 2.63 wt%. Island arc basalt (IAB), on the other hand, has the lowest TiO_2 content, approximately 0.98 wt%, whereas MORB contains about 1.5 wt% TiO_2 (Wilson, 1989). Within-plate basalts (WPB) display higher TiO_2 contents, ranging from 2.23 wt% to 2.9 wt% (Wilson, 1989). Regarding trace element abundances, IAB has significantly lower Nb and Ta contents, ranging from 1.7 to 2.7 μg/g and 0.1–0.18 μg/g, respectively. In comparison, WPB generally have elevated Nb and Ta concentrations, ranging from 13 to 84 μg/g and 0.73–5.9 μg/g, respectively (Peccerillo and Taylor, 1976). Characteristics of element ratios in basaltic rocks from various tectonic settings reveal that WPB and MORB are enriched in TiO_2 and HFSEs, and show special element ratios as following: Nb/La >0.8, Ti/Y > 350, Ti/V > 30, Hf/Ta <5, La/Ta <15, Th/Ta <3, and Ta/Yb < 0.1 (Peccerillo and Taylor, 1976; Condie, 1989). In contrast, IAB from active continental margins shows similar trends.

D1902 (amphibolite) and D1914 (gabbro) show a similar low TiO_2 content (average of 1.03 wt% and 1.13 wt%), which likes the continental arc basalts (CAB). But, the content of Nb and Ta is a little higher than CAB. The average trace element ratios of Nb/La (average of 0.52 and 0.87), Hf/Ta (average of 4.93 and 6.48), La/Ta (average of 21.46 and 18.35), Ti/Y (average of 328 and 344), Ti/V (average of 23.7 and 23.0), Th/Ta (average of 4.23 and 3.18), Zr/Y (average of 2.82 and 3.54), Ta/Yb = (average of 0.19 and 0.17) indicate that it is different from WPB and MORB but similar with CAB (Peccerillo and Taylor, 1976; Condie, 1989). These two mafic rocks also exhibit characteristics of island arc volcanic rocks in the La/Nb- Nb/Th diagram (Figure 8a). Furthermore, in the Nb/Yb-Th/Yb diagram, Hf/3-Th-Nb/16 and Hf/3-Th-Ta triangular diagram, these two mafic rocks fall within the continental arc and CAB area (Figures 8b–d). These characteristics suggest that D1902 (amphibolite) and D1914 (gabbro) were formed in an island arc environment.

The content of Nb (average = 15.8 μg/g) Ta (average = 1.13 μg/g) TiO_2 (average = 2.58 wt%) in D1905 (amphibolite) indicate a WPB setting. This may be attributed to the melt contamination, resulting in high contents. The ratios of Zr/Y (average = 4.75) and Ta/Yb (averages = 0.28) suggest a CAB setting, which is consistent with the La/Nb-Nb/Th diagram (Figure 8a). But the other average ratios of trace element Nb/La (average = 0.86), Hf/Ta (average = 4.84), La/Ta (average = 14.67), Ti/Y (average = 390), Ti/V (average = 40.3) and Th/Ta (average = 1.89) show the same characteristics with MORB. In the Hf/3-Th-Nb/16 and Hf/3-Th-Ta triangular diagram, this falls within the E-MORB area (Figures 8c,d). On the Nb/Yb-Th/Yb diagram, this sample distribute near the E-MORB (Figure 8b). These characteristics suggest D1905 (amphibolite) was formed in a mid-ocean ridge environment.

In D1911 (gabbro), the low content of TiO_2 (average = 1.02 wt%), Nb (average = 5.17 μg/g), Ta (average = 0.37 μg/g) and the average trace element ratios of Nb/La (average = 0.45), Hf/Ta (average = 5.44), La/Ta (average = 31.26) suggest an island arc setting (Figure 8a). But, the other average trace element ratios of Ti/Y = 359, Ti/V = 30.9, Th/Ta = 1.56, Zr/Y = 2.84 and Ta/Yb = 0.19 suggest a MORB feature, which is consistent with the results in tectonic setting patterns (Figures 8b–d). So, D1911 (gabbro) was formed in a mid-ocean ridge environment.

The tectonic nature of the Jiao-Liao-Ji Belt (JLJB) has been a subject of ongoing debate. A group of researchers advocates a continental rift model based on the presence of bimodal volcanic rocks within the Liaohe Group and geochemical signatures of Paleoproterozoic granitoids. These studies propose that the JLJB originated through continental rifting, subsequent sedimentary deposition, and eventual tectonic reworking via subduction and collision (Zhang, 1988; Chen et al., 2003; Hao et al., 2004; Luo et al., 2004; Li et al., 2005; 2006; Lu et al., 2006; Zhang et al., 2010; Jiang, 2014; Zhai and Santosh, 2011; Zhao et al., 2005; 2011; 2012; Zhao and Zhai, 2013; Hu et al., 2014). In contrast, other researchers distinguish the northern and southern Liaohe Group as two distinct continental margins based on contrasting P-T-t paths and metamorphic grades. These studies interpret the JLJB as an amalgamation zone formed by collision between two independent terranes (Lu, 1996; He and Ye, 1998; Li et al., 2001; Li and Chen, 2014; Lu et al., 2006; Meng et al., 2014). Alternatively, some researchers propose a third arc-continent collisional model for the JLJB, supported by integrated petrological, structural, and paleogeothermal evidence. The formation of the JLJB is related to northward subduction of the Nangrim Block in the south (Bai, 1993; Zhao et al., 2005; 2012; Zhai and Santosh, 2011; 2013; Zhao and Zhai, 2013; Li et al., 2012; Li and Chen, 2014; Liu et al., 2015; Li et al., 2015a; b, 2019; Xu et al., 2018a; 2018b; Xu and Liu, 2019; Xu and Liu, 2019; Chen et al., 2017a; 2018; 2020a; 2020b; 2021; 2024). Our new geochemical data from the Lieryu mafic rocks reveal distinct arc and mid-ocean ridge settings, providing critical evidence for the existence of a Paleoproterozoic oceanic basin that underwent subduction-accretion processes. These findings collectively support the interpretation that the JLJB represents a collisional orogen formed during the closure of a Paleoproterozoic oceanic basin.

6 Conclusion

(1) Zircon U-Pb ages (2052 ± 15 Ma, 2089 ± 55 Ma, 2053 ± 28 Ma, 2,190 ± 13 Ma) have been obtained from mafic rocks in Lieryu Formation, which constrained the mafic magmatism to 2,190–1995 Ma. Combined with the geochronological results of felsic volcanic rocks, the formation age of the Lieryu Formation is limited to 2,229–1959 Ma. The overlapping age among Langzishan (2078–1952 Ma), Lieryu (2,229–1959 Ma), Gaojiayu (2,184–1928 Ma) and Dashiqiao (2054–2,171 Ma) formations reveals a disordered stratum.

(2) Geochemical characteristics reveal that the mafic rocks belong to the calc-alkaline series and originated from transitional mantle. The D1902 (amphibolite), D1905 (amphibolite) and D1911 (gabbro) are mainly influenced by melt metasomatism, while the D1914 (gabbro) has undergone dual metasomatism of fluid and melt in the source. The D1902 (amphibolite), D1905 (amphibolite) and D1914 (gabbro) are product of partial melting of amphibole-bearing spinel lherzolite, and the D1911 (gabbro) is product of partial melting of garnet–spinel lherzolite. During the ascent and emplacement, assimilation

and contamination occurred between mafic magmas and continental crustal materials.

(3) Characteristics of major and trace elements suggest that D1902 (amphibolite) and D1914 (gabbro) were formed in an island arc environment, and the D1905 (amphibolite) and D1911 (gabbro) were formed in a mid-ocean ridge environment. This indicates the existence of ancient oceans in the Paleoproterozoic and the JLJB was formed during the subduction and extinction process of the Paleoproterozoic ocean.

Data availability statement

The original contributions presented in the study are included in the article/Supplementary Material, further inquiries can be directed to the corresponding author.

Author contributions

JC: Writing – original draft, Formal Analysis, Project administration, Visualization, Data curation, Methodology, Validation, Resources, Investigation, Supervision, Software, Funding acquisition, Conceptualization, Writing – review and editing. LL: Writing – review and editing, Validation, Resources, Investigation, Methodology. BL: Methodology, Validation, Writing – review and editing, Investigation. YT: Methodology, Validation, Investigation, Writing – review and editing. CZ: Methodology, Writing – review and editing, Investigation, Validation. YaZ: Writing – review and editing, Investigation, Validation, Methodology. YZ: Methodology, Writing – review and editing, Investigation, Validation.

Funding

The author(s) declare that financial support was received for the research and/or publication of this article. This research was financially supported by the China Geological Survey (Grants DD20242927 and DD20190042) and the National Natural Science Foundation of China (Grant Nos 42302221 and U2244213).

Conflict of interest

Author YT was employed by Liaoning Geological and Mineral Survey Institute Co., Ltd.

The remaining authors declare that the research was conducted in the absence of any commercial or financial relationships that could be construed as a potential conflict of interest.

Generative AI statement

The author(s) declare that no Generative AI was used in the creation of this manuscript.

Publisher's note

All claims expressed in this article are solely those of the authors and do not necessarily represent those of their affiliated organizations, or those of the publisher, the editors and the reviewers. Any product that may be evaluated in this article, or claim that may be made by its manufacturer, is not guaranteed or endorsed by the publisher.

Supplementary material

The Supplementary Material for this article can be found online at: https://www.frontiersin.org/articles/10.3389/feart.2025.1592749/full#supplementary-material

References

Aldanmaz, E., Pearce, J. A., Thirlwall, M. F., and Mitchell, J. G. (2000). Petrogenetic evolution of late Cenozoic, post-collision volcanism in western Anatolia, Turkey. *J. Volcanol. Geotherm. Res.* 102, 67–95. doi:10.1016/s0377-0273(00)00182-7

Andersen, T. (2002). Correction of common lead in U-Pb analyses that do not report 204Pb. *Chem. Geol.* 192, 59–79. doi:10.1016/s0009-2541(02)00195-x

Bai, J. (1993). *The precambrian Geology and Pb-Zn mineralization in the northern margin of north China platform*. Beijing: Geological Publishing House, 1–136.

Belousova, E., Griffin, W., O'Reilly, S. Y., and Fisher, N. (2002). Igneous zircon: trace element composition as an indicator of source rock type. *Contributions Mineralogy Petrology* 143, 602–622. doi:10.1007/s00410-002-0364-7

Bi, J. H., Ge, W. C., Xing, D. H., Yang, H., Dong, Y., Tian, D. X., et al. (2018b). Palaeoproterozoic meta-rhyolite and meta-dacite of the Liaohe group, jiao-liao-ji belt, north China craton: petrogenesis and implications for tectonic setting. *Precambrian Res.* 314, 306–324. doi:10.1016/j.precamres.2018.06.007

Bi, J. H., Xing, D. H., Ge, W. C., Yang, H., and Wang, Z. H. (2018a). Age and tectonic setting of meta-acid volcanic rocks from the North Liaohe Group in the Liaodong area: Paleoproterozoic intracontinental rift or active continental margin? *Earth Sci. Front.* 25 (3), 295–308.

Bureau of Geology and Mineral Resources of Liaoning Province (2014). *Regional Geology of liaoning Province*. Beijing: Geological Publishing House, 595–763. (in Chinese).

Chen, B., Li, Z., Wang, J. L., Yang, F., Liu, C., and Zhao, Y. (2016). Liaodong Peninsula ~2.2 Ga magmatic event and its geological significance. *J. Jilin Univ. Earth Sci. Ed.* 46 (2), 303–320.

Chen, J., Tian, Y., Gao, Z., Li, B., Zhao, C., Li, W., et al. (2024). Geochronology and geochemistry of Paleoproterozoic mafic rocks in northern Liaoning and their geological significance. *Minerals* 14, 717. doi:10.3390/min14070717

Chen, J. S., An, M. G., Duan, M., Li, W., and Liu, Y. (2017b). The age of the Dashiqiao Formation in the Liaohe Group: constraints from LA-ICP-MS zircon U-Pb dating of acidic volcanic rocks. *Geol. Resour.* 26 (2), 105–110.

Chen, J. S., Jiang, Z. Q., Li, W. W., Li, B., Liu, M., Yang, F., et al. (2018). The formation ages of the Langzishan and Lieryu formations in Lianshanguan area, Benxi, Liaoning province, and its geological significance. *Geol. Bull. China* 37, 1693–1703.

Chen, J. S., Li, W. W., Xing, D. H., Yang, Z. Z., Tian, D. X., Zhang, L. D., et al. (2020b). Zircon U-Pb geochronology of volcanic rocks from Gaojiayu Formation, Liaohe group, liaoning province and its geological significance. *Earth Sci.* 45, 3934–3949.

Chen, J. S., Tian, D. X., Xing, D. H., Li, B., Liu, M., Yang, F., et al. (2020a). Zircon U-Pb geochronology and its geological significance of the basic volcanic rocks from the Li'eryu Formation, Liaohe Group in Kuandian area. *Earth Sci.* 45, 3282–3294.

Chen, J. S., Xing, D. H., Liu, M., Li, B., Yang, H., Tian, D. X., et al. (2017a). Zircon U–Pb chronology and geological significance of felsic volcanic rocks in the Liaohe Group from the Liaoyang area, Liaoning Province. *Acta Petrol. Sin.* 33, 2792–2810.

Chen, J. S., Yang, Z. Z., Tian, D. X., Xing, D. H., Zhang, L. D., Yang, F., et al. (2021). Geochronological framework of Paleoproterozoic intrusive rocks and its constraints on tectonic evolution of the Liao-Ji Belt, Sino-Korean Craton. *J. Earth Sci.* 32, 8–24. doi:10.1007/s12583-020-1367-x

Chen, R. D., Li, X. D., and Zhang, F. S. (2003). Several problems about the Paleoproterozoic geology of eastern Liaodong. *Geol. China* 30 (2), 207–213.

Chi, Q. H., and Yan, M. C. (2007). *Handbook of elemental abundance for applied geochemistry*. Beijing: Geological Publishing House, 1–148. (in Chinese).

Condie, K. C. (1989). Geochemical changes in baslts and andesites across the Archean-Proterozoic boundary: identification and significance. *Lithos* 23, 1–18. doi:10.1016/0024-4937(89)90020-0

Condie, K. C., Frey, B. A., and Kerrich, R. (2002). The 1.75 Ga Iron King Volcanics in West Central Arizona: a remnant of an accreted oceanic plateau derived from a mantle plume with a deep depleted component. *Lithos* 64, 49–62. doi:10.1016/s0024-4937(02)00158-5

De la Roche, H., Leterrier, J., Grandclaude, P., and Marchal, M. (1980). A classification of volcanic and plutonic rocks using R1R2-diagram and major-element analyses—its relationships with current nomenclature. *Chem. Geol.* 29, 183–210. doi:10.1016/0009-2541(80)90020-0

Dong, Y., Bi, J. H., Xing, D. H., Liu, F. L., Tian, Z. H., Cai, J., et al. (2019). Geochronology and geochemistry of Liaohe group and liaoji granitoid in the jiao-liao-ji belt, north China craton: implications for petrogenesis and tectonic evolution. *Precambrian Res.* 332, 105399. doi:10.1016/j.precamres.2019.105399

Dupuy, C., and Dostal, J. (1984). Trace element geochemistry of some continental tholeiites. *Earth Planet. Sci. Lett.* 67, 61–69. doi:10.1016/0012-821x(84)90038-4

Gao, B. S., Dong, Y. S., Li, F. Q., Wang, P. S., Gan, Y. C., Chen, M. S., et al. (2017). Petrogenesis of the Lieryu Formation of the South Liaohe Group in the Huanghuadian area, Liaodong Peninsula. *Acta Petrologica Sinica* 33 (9), 2725–2742 (in Chinese).

Hao, D. F., Li, S. Z., Zhao, G. C., Sun, M., Han, Z. Z., and Zhao, G. T. (2004). Origin and its constraint to tectonic evolution of Paleoproterozoic granitoids in the eastern Liaoning and Jilin province, North China. *Acta Petrol. Sin.* 20 (6), 1409–1416.

He, G. P., and Ye, H. W. (1998). Two types of early Proterozoic metamorphism in the eastern Liaoning to southern Jilin and their tectonic implication. *Acta Petrol. Sin.* 14, 152–162.

Hoskin, P. W. O., and Ireland, T. R. (2000). Rare earth element chemistry of zircon and its use as a provenance indicator. *Geology* 28, 627–630. doi:10.1130/0091-7613(2000)028<0627:reecoz>2.3.co;2

Hu, G. Y., Li, Y. H., Fan, R. L., Wang, T. H., Fan, C. F., and Wang, Y. B. (2014). The forming age of the borate deposits in Kuandian area, eastern Liaoning Province: constraints from the SHRIMP U-Pb data and boron isotopic composition. *Acta Geol. Sin.* 88 (10), 1932–1943.

Jiang, C. C. (2014). Continental margin fold belt of Paleoproterozoic in Eastern Liaoning-Jilin—the formation and evolution of Kuandian-Caohe fold belt. *Geol. Rev.* 60 (3), 576–579. (in Chinese).

Jourdan, F., Bertrand, H., Schaerer, U., Blichert-Toft, J., Feraud, G., and Kampunzu, A. B. (2007). Major and trace element and Sr, Nd, Hf, and Pb isotope compositions of the Karoo large igneous province, Botswana-Zimbabwe: lithosphere vs mantle plume contribution. *J. Petrology* 48, 1043–1077. doi:10.1093/petrology/egm010

Kerrich, R., Polat, A., Wyman, D., and Hollings, P. (1999). Trace element systematics of Mg- to Fe-tholeiitic basalt suites of the Superior Province: implications for Archean mantle reservoirs and greenstone belt genesis. *Lithos* 46, 163–187. doi:10.1016/s0024-4937(98)00059-0

Li, S. Z., Han, Z. Z., Liu, Y. J., Zhao, G. C., Sun, M., and Wang, P. C. (2001). Regional metamorphism of the Liaohe group: implications for continental dynamics. *Geol. Rev.* 47, 9–18.

Li, S. Z., and Zhao, G. C. (2007). SHRIMP U-Pb zircon geochronology of the liaoji granitoids: constraints on the evolution of the paleoproterozoic jiao-liao-ji belt in the eastern block of the North China craton. *Precambrian Res.* 158, 1–16. doi:10.1016/j.precamres.2007.04.001

Li, S. Z., Zhao, G. C., Santosh, M., Liu, X., Dai, L. M., Suo, Y. H., et al. (2012). Paleoproterozoic structural evolution of the southern segment of the jiao-liao-ji belt, north China craton. *Precambrian Res.* 200–203, 59–73. doi:10.1016/j.precamres.2012.01.007

Li, S. Z., Zhao, G. C., Sun, M., Han, Z. Z., Liu, Y. J., Wang, Y. B., et al. (2005). Deformation history of the paleoproterozoic Liaohe assemblage in the eastern block of the North China craton. *J. Asian Earth Sci.* 24, 659–674. doi:10.1016/j.jseaes.2003.11.008

Li, S. Z., Zhao, G. C., Sun, M., Liu, Y. J., Han, Z. Z., and Wilde, S. A. (2006). Are the South and North Liaohe groups of north China craton different exotic terranes? Nd isotope constraints. *Gondwana Res.* 9, 198–208. doi:10.1016/j.gr.2005.06.011

Li, Z., and Chen, B. (2014). Geochronology and geochemistry of the paleoproterozoic metabasalts from the jiao-liao-ji belt, north China craton: implications for petrogenesis and tectonic setting. *Precambrian Res.* 255, 653–667. doi:10.1016/j.precamres.2014.07.003

Li, Z., Chen, B., Liu, J. W., Wei, C. J., Yan, X., and Gong, M. Y. (2015a). Zircon U-Pb ages and their implications for the South Liaohe group in the Liaodong peninsula, northeast China. *Acta Petrol. Sin.* 31 (6), 1589–1605.

Li, Z., Chen, B., Wei, C. J., Yan, X., Fu, B., and Gong, M. Y. (2015b). Provenance and tectonic setting of the Paleoproterozoic metasedimentary rocks from the Liaohe Group, Jiao-Liao-Ji Belt, North China Craton: insights from detrital zircon U-Pb geochronology, whole-rock Sm-Nd isotopes, and geochemistry. *J. Asian Earth Sci.* 111, 711–732. doi:10.1016/j.jseaes.2015.06.003

Li, Z., Chen, B., and Yan, X.(2018). The Liaohe Group: an insight into the Paleoproterozoic tectonic evolution of the Jiao–Liao–Ji Belt, North China Craton. *Precambrian Resserach*. doi:10.1016/j.precamres.2018.01.009

Li, Z., Chen, B., and Yan, X. (2019a). The Liaohe group: an insight into the paleoproterozoic tectonic evolution of the jiao-liao-ji belt, north China craton. *Precambrian Res.* 326, 174–195. doi:10.1016/j.precamres.2018.01.009

Li, Z., Meng, E., Wang, C. Y., and Li, Y. G. (2019b). Early precambrian tectono-thermal events in southern Jilin province, China: implications for the evolution of neoarchean to paleoproterozoic crust in the northeastern north China craton. *Mineralogy Petrology* 113, 185–205. doi:10.1007/s00710-018-0649-9

Li, Z., and Wei, C. J. (2017). Two types of Neoarchean basalts from Qingyuan greenstone belt, North China Craton: petrogenesis and tectonic implications. *Precambrian Res.* 292, 175–193. doi:10.1016/j.precamres.2017.01.014

Li, Z., Wei, C. J., Chen, B., Fu, B., and Gong, M. Y. (2020). Late neoarchean reworking of the mesoarchean crustal remnant in northern liaoning, north China craton: a U-Pb-Hf-O-Nd perspective. *Gondwana Res.* 80, 350–369. doi:10.1016/j.gr.2019.10.020

Liu, F. L., Liu, P. H., Wang, F., Liu, C. H., and Cai, J. (2015). Progresses and overviews of voluminous meta-sedimentary series within the Paleoproterozoic Jiao-Liao-Ji orogenic/mobile belt, North China Craton. *Acta Petrol. Sin.* 31, 2816–2846.

Liu, J., Zhang, J., Liu, Z. H., Yang, F., Wang, Y., Tan, H. Y., et al. (2018). Geochemical and geochronological study on the Paleoproterozoic rock assemblage of the Xiuyan region: new constraints on an integrated rift-and-collision tectonic process involving the evolution of the Jiao-Liao-Ji Belt, North China Craton. *Precambrian Res.* 310, 179–197. doi:10.1016/j.precamres.2018.03.005

Liu, P. H., Cai, J., and Zou, L. (2017). Metamorphic P-T-t path and its geological implication of the Sanjiazi garnet amphibolites from the northern Liaodong Peninsula, Jiao-Liao-Ji Belt: constraints on phase equilibria and zircon U-Pb dating. *Acta Petrol. Sin.* 33, 2649–2674.

Liu, P. H., Liu, F. L., Tian, Z. H., Yang, H., Cai, J., and Shi, Y. (2019). Petrological and geochronological evidence for paleoproterozoic granulite-facies metamorphism of the South Liaohe group in the jiao-liao-ji belt, north China craton. *Precambrian Res.* 332, 105406. doi:10.1016/j.precamres.2019.105406

Lu, L. Z. (1996). The Precambrian metamorphic geology and tectonic evolution of the Jiao-Liao massif. *J. Changchun Univ. Earth Sci.* 26, 25–32.

Lu, X. P., Wu, F. Y., Guo, J. H., Zhao, G. C., Sun, M., Wilde, S. A., et al. (2006). Zircon U-Pb geochronological constraints on the paleoproterozoic crustal evolution of the eastern block in the North China craton. *Precambrian Res.* 146, 138–164. doi:10.1016/j.precamres.2006.01.009

Ludwig, K. R. (2003). *User's manual for Isoplot 3.0: a geochronological toolkit for microsoft excel*, 75. Berkeley: Berkeley Geochronology Center Special Publication.

Luo, Y., Sun, M., Zhao, G. C., Wilde, S. A., Li, S. Z., Han, Z. Z., et al. (2004). LA-ICP-MS U-Pb zircon ages of the Liaohe group in the eastern block of the North China craton: constraints on the evolution of the jiao-liao-ji belt. *Precambrian Res.* 134, 349–371. doi:10.1016/j.precamres.2004.07.002

Luo, Y., Sun, M., Zhao, G. C., Wilde, S. A., Li, S. Z., Han, Z. Z., et al. (2008). A comparison of U-Pb and Hf isotopic compositions of detrital zircons from the North and South Liaohe groups: constraints on the evolution of the jiao-liao-ji belt, north China craton. *Precambrian Res.* 163, 279–306. doi:10.1016/j.precamres.2008.01.002

McKenzie, D., and O'Nions, R. K. (1991). Partial melt distributions from inversion of rare earth element concentrations. *J. Petrol.* 32, 1021–1091. doi:10.1093/petrology/32.5.1021

Meng, E., Liu, F. L., Liu, P. H., Liu, C. H., Yang, H., Wang, F., et al. (2014). Petrogenesis and tectonic significance of Paleoproterozoic meta-mafic rocks from central Liaodong Peninsula, northeast China: evidence from zircon U-Pb dating and *in situ* Lu-Hf isotopes, and whole-rock geochemistry. *Precambrian Res.* 247, 92–109. doi:10.1016/j.precamres.2014.03.017

Meng, E., Wang, C. Y., Li, Y. G., Li, Z., Yang, H., Cai, J., et al. (2017). Zircon U-Pb-Hf isotopic and whole-rock geochemical studies of Paleoproterozoic metasedimentary rocks in the northern segment of the Jiao-Liao-Ji Belt, China: implications for provenance and regional tectonic evolution. *Precambrian Res.* 298, 472–489. doi:10.1016/j.precamres.2017.07.004

Middlemost, E. A. K. (1994). Naming materials in the magma/igneous rock system. *Earth-Sci. Rev.* 37, 215–224. doi:10.1016/0012-8252(94)90029-9

Mo, X. X. (2019). Magmatism and deep geological process. *Earth Sci.* 44 (5), 1487–1493.

Pearce, J. A. (1982). "Trace elements characteristic of lavas from destructive plate boundaries," in *Andesites. Orogenic andesites and related rocks*. Editor R. S. Thorpe (Chichester, UK: John Wiley & Sons), 525–548.

Pearce, J. A. (1996). "A user's guide to basalt discrimination diagrams," in *Trace element geochemistry of volcanic rocks: applications for massive sulphide exploration. Short course notes*. Editor D. A. Wyman (Ottawa, Canada: Geological Association of Canada: St. John's, NL, Canada), 12, 79–113.

Peccerillo, A., and Taylor, S. R. (1976). Geochemistry of Eocene calc-alkaline volcanic rocks from the Kastamonu area, northern Turkey. *Contrib. Mineral. Petrol.* 58, 63–81. doi:10.1007/bf00384745

Peng, P., Wang, C., Wang, X. P., and Yang, S. Y. (2015). Qingyuan high-grade granite-greenstone terrain in the eastern north China craton: root of a neoarchaean arc. *Tectonophysics* 662, 7–21. doi:10.1016/j.tecto.2015.04.013

Plank, T., and Langmuir, C. H. (1998). The chemical composition of subducting sediment and its consequences for the crust and mantle. *Chem. Geol.* 145, 325–394. doi:10.1016/s0009-2541(97)00150-2

Rollinson, H. R. (1993). *Using geochemical data*. London: Longman, 1–352.

Sajona, F. G., Maury, R. C., Pubellier, M., Leterrier, J., Bellon, H., and Cotton, J. (2000). Magmatic source enrichment by slab-derived melts in a young post-collision setting, Central Mindanao (Philippines). *Lithos* 54, 173–206. doi:10.1016/s0024-4937(00)00019-0

Sklyarov, E. V., Gladkochub, D. P., Mazukabzov, A. M., Menshagin, Y. V., Watanabe, T., and Pisarevsky, S. A. (2003). Neoproterozoic mafic dike swarms of the Sharyzhalgai metamorphic massif, southern Siberian Craton. *Precambrian Res.* 122, 359–376. doi:10.1016/s0301-9268(02)00219-x

Sun, S. S., and McDonough, W. F. (1989). Chemical and isotopic systematics of oceanic basalts: implications for mantle composition and processes. *Geol. Soc. Lond. Spec. Publ.* 42, 313–345. doi:10.1144/gsl.sp.1989.042.01.19

Sun, S. S., and Nesbitt, R. W. (1978). Geochemical regularities and genetic significance of ophiolitic basalts. *Geology* 6, 689–693. doi:10.1130/0091-7613(1978)6<689:gragso>2.0.co;2

Tian, Z. H., Liu, F. L., Windley, B. F., Cai, J., Wang, W., Zhang, M., et al. (2017). Polyphase structural deformation of low-to medium-grade metamorphic rocks of the Liaohe group in the jiao-liao-ji orogenic belt, north China craton: correlations with tectonic evolution. *Precambrian Res.* 303, 641–659. doi:10.1016/j.precamres.2017.08.017

Wan, Y. S., Song, B., Yang, C., and Liu, D. Y. (2005). Zircon SHRIMP U-Pb geochronology of Archaean rocks from the Fushun-Qingyuan area, Liaoning province and its geological significance. *Acta Geol. Sin.* 79, 78–87.

Wiedenbeck, M., Allé, P., Corfu, F., Griffin, W. L., Meier, M., Oberli, F., et al. (1995). Three natural zircon standards for U-Th-Pb, Lu-Hf, trace element and REE analyses. *Geostand. Newsl.* 19, 1–23.

Wilson, M. (1989). *Igneous petrogenesis: a global tectonic approach*. London, UK: Unwin Hyman, 1–466.

Woodhead, J. D., Hergt, J. M., Davidson, J. P., and Eggins, S. M. (2001). Hafnium isotope evidence for conservative element mobility during subduction zone processes. *Earth Planet. Sci. Lett.* 192, 331–346. doi:10.1016/s0012-821x(01)00453-8

Wu, F. Y., Li, X. H., Yang, J. H., and Zheng, Y. F. (2007). Discussions on the petrogenesis of granites. *Acta Petrol. Sin.* 23, 1217–1238.

Xu, W., and Liu, F. L. (2019). Geochronological and geochemical insights into the tectonic evolution of the paleoproterozoic jiao-liao-ji belt, sino-Korean craton. *Earth-Science Rev.* 193, 162–198. doi:10.1016/j.earscirev.2019.04.019

Xu, W., Liu, F. L., and Liu, C. H. (2017). Petrogenesis and geochemical characteristics of the North Liaohe metabasic rocks, Jiao-Liao-Ji orogenic belt and their tectonic significance. *Acta Petrol. Sin.* 33 (9), 2743–2757.

Xu, W., Liu, F. L., Santosh, M., Liu, P. H., Tian, Z. H., and Dong, Y. S. (2018a). Constraints of mafic rocks on a paleoproterozoic back-arc in the jiao-liao-ji belt, north China craton. *J. Asian Earth Sci.* 166, 195–209. doi:10.1016/j.jseaes.2018.06.016

Xu, W., Liu, F. L., Tian, Z. H., Liu, L. S., Ji, L., and Dong, Y. S. (2018b). Source and petrogenesis of paleoproterozoic meta-mafic rocks intruding into the North Liaohe group: implications for back-arc extension prior to the formation of the jiao-liao-ji belt, north China craton. *Precambrian Res.* 307, 66–81. doi:10.1016/j.precamres.2018.01.011

Xu, W., Liu, F. L., Wang, F., Tian, Z. H., Liu, P. H., and Dong, Y. S. (2019). Paleoproterozoic tectonic evolution of the jiao-liao-ji belt, north China craton: geochemical and isotopic evidence from ca. 2.17 Ga felsic tuff. *Geol. J.* 54, 1–20. doi:10.1002/gj.3380

Zhai, M. G., and Santosh, M. (2011). The early Precambrian odyssey of the North China Craton: a synoptic overview. *Gondwana Res.* 20 (1), 6–25. doi:10.1016/j.gr.2011.02.005

Zhai, M. G., and Santosh, M. (2013). Metallogeny of the North China craton: link with secular changes in the evolving earth. *Gondwana Res.* 24 (1), 275–297. doi:10.1016/j.gr.2013.02.007

Zhang, Q. S. (1988). Early Proterozoic tectonic styles and associated mineral deposits of the North China platform. *Precambrian Res.* 39 (1-2), 1–29. doi:10.1016/0301-9268(88)90047-2

Zhang, Q. S., and Yang, Z. S. (1988). *Early crust and mineral deposits of Liaodong peninsula*. Beijing: China. Geological Publishing House, 1–575.

Zhang, W., Liu, F. L., Cai, J., Tian, Z. H., Liu, L. S., Ji, L., et al. (2018). Geochemistry, zircon U-Pb dating and tectonic implications of the palaeoproterozoic ji'an and laoling groups, northeastern jiao-liao-ji belt, north China craton. *Precambrian Res.* 314, 264–287. doi:10.1016/j.precamres.2018.06.010

Zhang, X. H., Yuan, L. L., Xue, F. H., and Zhang, Y. B. (2012). Contrasting Triassic ferroan granitoids from northwestern Liaoning, North China: magmatic monitor of Mesozoic decratonization and a craton–orogen boundary. *Lithos* 144-145, 12–23. doi:10.1016/j.lithos.2012.03.022

Zhang, Y. F., Liu, J. D., Xiao, R. G., Wang, S. Z., Wang, J., and Bao, D. J. (2010). The Hyalotourmalites of Houxianyu borate deposit in eastern Liaoning: zircon features and SHRIMP dating. *Earth Science—Journal China Univ. Geosciences* 35 (6), 985–999.

Zhang, Y. M., Pei, X. Z., Li, Z. C., Li, R. B., Liu, C. J., Pei, L., et al. (2019). Zircon U-Pb geochronology, geochemistry and its geological implication of the early Indosinian basic complex in the Qinghai Nanshan tectonic belt. *Earth Sci.* 44 (8), 2461 –2477.

Zhao, G. C., Cao, L., Wilde, S., Sun, M., Choe, W., and Li, S. Z. (2006). Implications based on the first SHRIMP U–Pb zircon dating on Precambrian granitoid rocks in North Korea. *Earth Planet. Sci. Lett.* 251 (3-4), 365–379. doi:10.1016/j.epsl.2006.09.021

Zhao, G. C., Cawood, P. A., Li, S. Z., Wilde, S. A., Sun, M., Zhang, J., et al. (2012). Amalgamation of the North China craton: key issues and discussion. *Precambrian Res.* 222-223, 55–76. doi:10.1016/j.precamres.2012.09.016

Zhao, G. C., Li, S. Z., Sun, M., Wilde, S. A., Liu, J., and Wu, C. M. (2011). Assembly, accretion, and break-up of the Palaeo-Mesoproterozoic Columbia supercontinent: record in the North China Craton revisited. *Int. Geol. Rev.* 53 (11-12), 1331–1356. doi:10.1080/00206814.2010.527631

Zhao, G. C., Sun, M., Wilde, S. A., and Li, S. Z. (2005). Late archean to paleoproterozoic evolution of the North China craton: key issues revisited. *Precambrian Res.* 136 (3-4), 177–202. doi:10.1016/j.precamres.2004.10.002

Zhao, G. C., and Zhai, M. G. (2013). Lithotectonic elements of precambrian basement in the North China craton: review and tectonic implications. *Gondwana Res.* 23 (4), 1207–1240. doi:10.1016/j.gr.2012.08.016

Zhao, Y., Kou, L. L., Zhang, P., Bi, Z. W., Li, D. T., and Chen, C. (2019). Characteristics of geochemistry and Hf isotope from meta-gabbro in longchang area, Liaodong peninsula: implications on evolution of the jiao-liao-ji paleoproterozoic orogenic belt. *Earth Sci.* 44 (10), 3333–3345.